Trajectory Design for UAV-Enabled Multiuser Wireless Power Transfer with Nonlinear Energy Harvesting

Xiaopeng Yuan, Tianyu Yang, Yulin Hu∗, Jie Xu, and Anke Schmeink

Abstract

In this paper, we study an unmanned aerial vehicle (UAV)-enabled multiuser wireless power transfer (WPT) network, where a UAV is responsible for providing wireless energy for a set of ground devices (GDs) deployed in an area. We focus on the design of UAV trajectory subject to the maximum flight speed limit, in order to maximize the minimum harvested energy among GDs over a particular charging duration. Different from prior works that considered simplified linear energy harvesting models, this paper for the first time takes into account the realistic nonlinear energy harvesting model for the UAV trajectory design. However, the formulated trajectory design problem is highly non-convex and has infinite number of variables, thus making it be challenging to be solved optimally. To tackle this difficulty, we adopt the following three-step approach to obtain an efficient solution. First, we rigorously characterize that the optimal trajectory follows a new successive-hover-and-fly (SHF) structure, where the UAV hovers at a certain set of points for efficiently transferring energy, and flies among these hovering points with the maximum speed following certain arcs (not necessarily straight lines). Next, based on this SHF structure, we transform the original problem to a new one for finding a set of turning point variables during the maximum-speed flight, at which the UAV changes the flight direction without hovering. Finally, we use the techniques of convex approximation to solve the transformed problem. According to the convexity of the nonlinear energy harvesting model, we iteratively solve a

This work was supported in part by DFG (No. SCHM 2643/16), the National Key R&D Program of China (No. 2018YFB1800800), the Natural Science Foundation of China (No. 61871137), and the Guangdong Province Key Area R&D Program (No. 2018B030338001).

∗Y. Hu is the corresponding author, he is with School of Electronic Information, Wuhan University, 430072 Wuhan, China and ISEK Research Area, RWTH Aachen University, D-52074 Aachen, Germany, (Email: $yulin.hu$@ieee.org).

X. Yuan, and A. Schmeink are with ISEK Research Area, RWTH Aachen University, D-52074 Aachen, Germany. (email: {yuan, schmeink}@isek.rwth-aachen.de).

T. Yang is with Communications and Information Theory Group, TU Berlin, D-10587 Berlin, Germany (Email: tianyu.yang@tu-berlin.de).

J. Xu is with the Future Network of Intelligence Institute (FNii) and the School of Science and Engineering, The Chinese University of Hong Kong, Shenzhen, Shenzhen 518172, China (e-mail: xujie@cuhk.edu.cn).

series of convex optimization problems to update the UAV trajectory towards a high-quality solution. Numerical results show the convergence of the proposed approach, and validate its performance gain over conventional designs.

Index Terms

Unmanned aerial vehicle (UAV), nonlinear energy harvesting (EH), multiple users, energy fairness, trajectory optimization, successive-hover-and-fly (SHF).

I. Introduction

Nowadays, unmanned aerial vehicles (UAVs) have shown tremendous potentials in various applications (such as filming, aerial delivery, and wireless platforms), due to the high mobility in three-dimensional (3D) space and high controllability. Among others, UAV-enabled communication networks are particularly appealing. By exploiting the high mobility of UAVs and the high probability of aerial-to-ground line-of-sight links, the UAV-enabled wireless networks are expected to achieve improved communication performance than the traditional terrestrial networks [1]. Thanks to the controllable mobility, the UAV-enabled wireless networks actually provide an additional degree of freedom for the system operation and design [2] via adjusting UAVs' deployment locations and trajectories. For instance, by employing the UAV as a base station, the UAV deployment optimization has been discussed in [3]–[5] for providing the maximum coverage for ground users, and the UAV trajectory is optimized for maximizing the capacity [6] and energy efficiency [8]. In addition, by exploring the UAV as a mobile relay, the UAV trajectory design has been exploited for throughput maximization [9]. Furthermore, the trajectory optimization is also considered in UAV-enabled heterogeneous networks for capacity maximization [10], UAV-enabled data collection systems for energy efficiency maximization [11], and UAV-assisted data offloading systems [12].

On the other hand, integrating wireless power transfer (WPT) technologies [13] into communication networks is prominent to prolong the lifetime of low-power rechargeable sensor/devices (see, e.g., [14], [15]). Recently, using UAVs as energy transmitters for energy supply, namely UAV-enabled WPT, has been studied in [16]–[20], where a single UAV flying in the sky provides wireless energy towards electronic devices on the ground. In the literature, there have been some prior works investigating the trajectory design for UAV-enabled WPT [16]–[18] and UAV-enabled wireless powered communication networks (WPCN) [19], [20]. In particular, the authors in [16] investigated the UAV trajectory optimization problem to maximize the minimum radio-frequency

(RF) energy transferred to a set of ground devices (GDs), subject to the maximum UAV flight speed constraints. In [16], the authors solved the trajectory optimization problem by first obtaining a multi-location-hovering solution for the ideal case with UAV speed constraints ignored, and then proposing a suboptimal successive-hover-and-fly (SHF) trajectory design, where the UAV hovers above a set of points over time and flies *straightly* around these points at the maximum speed. Building upon [16], [17] studies a simplified one-dimensional (1D) UAV-enabled WPT network with GDs deployed in a line on the ground. Under the 1D setup, [17] for the first time characterized that the optimal 1D UAV trajectory must follow SHF structure, and accordingly proposed the optimal solution to the min-energy maximization problem based on the optimal structure. However, the trajectory design strategy in [17] is only applicable in the 1D topology. How to characterize the optimal UAV trajectory structure in a more general two-dimensional (2D) topology has not been addressed in the literature yet.

Furthermore, in the existing literature on UAV-enabled WPT or WPCN [16]–[20], the authors normally considered the RF energy as the performance metric by ignoring the energy harvesting (EH) process [21], or assumed the simplified linear EH models at the GDs [22], [23], [25]. It has been shown that under different input power and signal waveforms, the EH (or RF-to-direct current (DC) conversion) efficiency may vary dramatically (see, e.g., [26]). In particular, it has been shown in [27], [28] that the EH is a nonlinear process. The authors in [28]–[30] have made efforts to model and involve the nonlinearity in the study, while the introduced EH model is curve fitting based on a set of statistical results, i.e., the accuracy of such statistical model is lacking of essential analytical proof/guarantee. Fortunately, the authors in [27] rigorously derive this nonlinear EH process, which provides the analytical insights. To the best of our knowledge, the UAV trajectory design considering the realistic accurate nonlinear EH process is missing, thus motivating our investigation in this paper.

In this work, we provide an efficient UAV trajectory design for a UAV-enabled WPT network with a 2D topology, by taking into account the nonlinearity of the EH process at GDs. To efficiently and fairly charge these GDs, we aim at maximizing the minimum harvested DC energy among GDs by designing the UAV trajectory subject to a maximum flying speed constraint. The UAV trajectory design problem contains infinite number of variables over continuous time, and thus is difficult to be solved optimally. We provide an efficient approach to solve this difficult problem, with the main results summarized in the following.

- **Characterization of optimal UAV trajectory structure:** First, we rigorously prove that the

optimal UAV trajectory solution in a 2D scenario follows a new SHF structure, where the UAV should hover at a set of positions over time, and fly among these positions following certain arcs (instead of straightly) at the maximum speed. In addition, the upper bound of the number of hovering points is also derived.

- **Problem transformation based on turning points:** Next, to facilitate the solution, we introduce a sequence of turning points into the UAV's maximum-speed flight paths (arcs), such that any UAV flight paths can be approximated as a connection of line segments. By using the turning points together with the revealed optimal SHF structure, we transform the original min-energy maximization problem to a simplified one with finite number of variables, including the hovering positions and durations, and the positions of turning points during the maximum-speed flight.
- **Proposed solution via convex approximation:** Then, we use the technique of convex approximation to solve the transformed problem in an iterative manner. In each iteration, we approximate the harvested energy as a concave function with respect to UAV positions at a local point. By solving a series of approximated convex problems, the local points are updated towards a converged solution. In addition, we also present the initial trajectory design and analyze the computational complexity for this iterative algorithm.
- **Numerical results:** Finally, simulation results are presented to evaluate the performance of our proposed trajectory design. It is shown that the proposed design outperforms the conventional designs under linear EH models, and performs close to the performance upperbound when the flying speed is ignored.

The rest of this paper is organized as follows. In Section II, the system model is described together with a nonlinear EH model, based on which the min-energy minimization problem is formulated. Then, the optimal trajectory structure is proved in Section III. Based on the optimal structure, an iterative algorithm is proposed in Section IV. Finally, we provide our simulation results in Section V and conclude this work in Section VI.

II. System Model

We consider a UAV-enabled WPT system where K GDs are deployed in an area. We denote the fixed horizontal position of GD k by $(w_{x,k}, w_{y,k}), k \in \mathcal{K} \triangleq \{1, 2, \cdots, K\}$, where the knowledge of all these fixed positions are *a-priori* known by the UAV. In addition, we assume that the UAV flies at a fixed altitude $H > 0$. The charging process is executed within a period $\mathcal{T} \triangleq [0, T]$

with duration $T > 0$, where T is a constant that is properly set based on the available energy in UAV's battery and the maximum consumption power of UAV, such that the UAV can return to be recharged before the energy is used up. The horizontal location of UAV at time t is denoted by $(x(t), y(t))$, which is a variable to be optimized later. In addition, the maximal speed of the UAV is given by V. Hence, we have $(\dot{x}(t))^2 + (\dot{y}(t))^2 \leq V^2, \forall t \in \mathcal{T}$, where $\dot{x}(t)$ and $\dot{y}(t)$ respectively denote the first-derivatives of $x(t)$ and $y(t)$ with respect to t.

In practice, the wireless channels between the UAV and GDs are generally LoS-dominant. For facilitation, we assume a free space channel model by setting the path loss exponent to be two for all channels between the UAV and GDs. At time t, the channel gain from the UAV to GD $k \in \mathcal{K}$ is denoted as $h_k(x(t), y(t)) = \frac{\beta_0}{\left(x(t)-w_{x,k}\right)^2+\left(y(t)-w_{y,k}\right)^2+H^2}$, where the distance between the UAV and GD k is $\sqrt{(x(t)-w_{x,k})^2 + (y(t)-w_{y,k})^2 + H^2}$ and β_0 is the channel power gain at a reference distance of unit meter. Hence, the received RF power by GD k at time t is given by

$$Q_k\left(x(t), y(t)\right) = \frac{\beta_0 P}{\left(x(t)-w_{x,k}\right)^2+\left(y(t)-w_{y,k}\right)^2+H^2}, \tag{1}$$

where P is the constant transmit power of the UAV for WPT.

The received RF signal is further converted into the DC signal for charging the rechargeable battery at each GD. Different from existing works considering simplified linear EH models [16]–[20], in this work, we consider a practical non-linear EH (RF-to-DC conversion) model [27]. Due to the significant path loss and a relatively long distance from the UAV to GDs in WPT, the wireless signal received by GDs is generally attenuated in a large degree, so that the saturation power cannot be reached. Thus, we apply a small signal model [31] to process the non-linearity of rectifier (diode) during the charging at GDs. By applying a Taylor expansion of non-linearity in diode, the nonlinear relation between output charged current I_{out} and the received RF power Q can be characterized by an implicit function $I_{\text{out}}(Q)$. According to Eq.(6) in [32], we have

$$e^{\frac{R_{\text{L}} I_{\text{out}}(Q)}{n v_t}} \left(I_{\text{out}}(Q) + I_{\text{s}}\right) \approx \sum\nolimits_{j=0}^{n_o'} \alpha_j Q^j, \tag{2}$$

where R_L, n, v_t and I_s respectively denote the load resistance, the ideality factor, the thermal voltage and the reverse bias saturation current at diode. Here, the truncation order n_o' can be any positive integer, a larger value of which represents a more accurate nonlinear model. Moreover, all the α_j factors are obtained from the Taylor expansion and are definitely positive. Note that the charged (or harvested DC) power P_{ch} is clearly a function of output current $I_{\text{out}}(Q)$, given by $P_{\text{ch}} = [I_{\text{out}}(Q)]^2 R_L$, which implies that the charged power P_{ch} is also an implicit nonlinear

function of received power Q, denoted by $\mathcal{F}_{nl}(Q)$. Thus, for GD k the relationship between the harvested DC power $P_{ch,k}$ and the received RF power Q_k is expressed as

$$P_{ch,k} = \mathcal{F}_{nl}(Q_k) \triangleq [I_{\text{out}}(Q_k)]^2 R_L. \tag{3}$$

Although being implicit, the convexity of the nonlinear process $\mathcal{F}_{nl}$ has been proved in [32]. In particular, by letting $u = (x(t)-w_{x,k})^2+(y(t)-w_{y,k})^2$, Q_k given in (1) can be further expressed by $Q_k = Q_k(u) = \frac{\beta_0 P}{u+H^2}$. In addition, let $\dot{Q}_k(u)$ and $\ddot{Q}_k(u)$ represent the first and second derivatives of $Q_k(u)$ to u. Then, the following inequality holds

$$\ddot{Q}_k(u)Q_k(u) - \left(\dot{Q}_k(u)\right)^2 = \left(\frac{2\beta_0 P}{(u+H^2)^3}\right)\cdot\frac{\beta_0 P}{u+H^2} - \left(-\frac{\beta_0 P}{(u+H^2)^2}\right)^2 = \frac{\beta_0^2 P^2}{(u+H^2)^4} > 0. \tag{4}$$

According to [32], $\ddot{Q}_k(u)Q_k(u) - \left(\dot{Q}_k(u)\right)^2 \geq 0$ is a sufficient condition making $\mathcal{F}_{nl}(Q_k(u))$ be convex with respect to u. In other words, in the system considered in our work, $P_{ch,k} = \mathcal{F}_{nl}(Q_k(u)) = \mathcal{F}_{nl}\left(Q_k\left(x(t), y(t)\right)\right)$ is convex in $(x(t)-w_{x,k})^2+(y(t)-w_{y,k})^2$.

Due to the broadcast nature of wireless transmission, all GDs can simultaneously receive wireless power for EH during the whole charging period $\mathcal{T}$. As a result, the total harvested energy at GD k is given by

$$E_k(\{x(t), y(t)\}) = \int_0^T \mathcal{F}_{nl}(Q_k\left(x(t), y(t)\right))dt, \tag{5}$$

which is the key EH performance metric for evaluating the WPT process to GD k. Note that there are in total K GDs to be charged in the network. Taking the fairness issue into account, our objective is to design the UAV trajectory for maximizing the minimal harvested energy among all the K GDs during the charging period $\mathcal{T}$. The problem of interest is formulated as

$$(\text{OP}): \max_{\{x(t),y(t)\}} \min_{k\in\mathcal{K}} \int_0^T \mathcal{F}_{nl}(Q_k(x(t), y(t)))dt \tag{6a}$$

$$\text{s.t.} \quad (\dot{x}(t))^2 + (\dot{y}(t))^2 \leq V^2, \forall t \in \mathcal{T}. \tag{6b}$$

By introducing an auxiliary variable E, the original problem (OP) is equivalently reformulated as

$$(\text{P1}): \max_{\{x(t),y(t)\},E} \quad E \tag{7a}$$

$$\text{s.t.} \quad \int_0^T \mathcal{F}_{nl}(Q_k(x(t), y(t)))dt \geq E, \forall k \in \mathcal{K}. \tag{7b}$$

$$(\dot{x}(t))^2 + (\dot{y}(t))^2 \leq V^2, \forall t \in \mathcal{T}. \tag{7c}$$

Notice that both the original problem (OP) and the reformulated problem (P1) are non-convex, due to the fact that the objective function in (OP) is non-concave, and constraint (7b) in (P1)

is non-convex. Furthermore, both problems contain an infinite number of variables $\{x(t), y(t)\}$ over continuous time, which makes the optimization problem difficult to be solved optimally. In addition, the nonlinear process $\mathcal{F}_{nl}$ is indeed an implicit function [32]. Therefore, the solution remains to be extremely challenging to be found.

III. Structure of Optimal Trajectory

In this section, we characterize the structure of the optimal trajectory solution of problem (OP). It is worthwhile to mention that the structure in [17] is just a special case of that in this work when the linear EH is considered in the 1D scenario.

We have two key lemmas addressing the structure of an optimal trajectory of problem (P1).

Lemma 1. *Consider a trajectory $\{x(t), y(t)\}$ satisfying the maximum speed constraint V and with time duration T and path/arc length d_p. We can always find two trajectories $\{\bar{x}(t), \bar{y}(t)\}$ and $\{\hat{x}(t), \hat{y}(t)\}$ jointly achieving the same WPT performance. $\{\bar{x}(t), \bar{y}(t)\}$ is a trajectory flying along the original path with maximum speed V in duration $\bar{T} = d_p/V$, while $\bar{T}$ is the corresponding time duration. $\{\hat{x}(t), \hat{y}(t)\}$ is limited on the original path, and has a time duration $\hat{T} = T - \bar{T}$ without any UAV speed constraints (speed-free). In other words, the following equality holds for any GD $k \in \mathcal{K}$.*

$$\int_0^T \mathcal{F}_{nl}(Q_k\left(x\left(t\right), y\left(t\right)\right))dt = \int_0^{\bar{T}} \mathcal{F}_{nl}(Q_k\left(\bar{x}\left(t\right), \bar{y}\left(t\right)\right))dt + \int_0^{\hat{T}} \mathcal{F}_{nl}(Q_k\left(\hat{x}\left(t\right), \hat{y}\left(t\right)\right))dt. \quad (8)$$

Proof. See Appendix A. □

For any optimal trajectory $\{x^\star(t), y^\star(t)\}$ of problem (P1), according to Lemma 1, we can split it into two trajectories (i.e., the maximum-speed one $\{\bar{x}^\star(t), \bar{y}^\star(t)\}$ and speed-free one $\{\hat{x}^\star(t), \hat{y}^\star(t)\}$), which can jointly achieve the same performance as $\{x^\star(t), y^\star(t)\}$. The details of obtaining the two trajectories from $\{x^\star(t), y^\star(t)\}$ are provided in the proof of Lemma 1 in Appendix A.

In trajectory $\{\bar{x}^\star(t), \bar{y}^\star(t)\}$, the UAV flies along the path of $\{x^\star(t), y^\star(t)\}$ with maximum speed V. For $\{\bar{x}^\star(t), \bar{y}^\star(t)\}$, the harvested energy by GD $k \in \mathcal{K}$ is given by

$$\bar{E}_k^\star = \int_0^{\bar{T}} \mathcal{F}_{nl}(Q_k(\bar{x}^\star(t), \bar{y}^\star(t)))dt. \quad (9)$$

As the trajectory $\{x^\star(t), y^\star(t)\}$ is the optimal solution of problem (P1), it can be shown that the speed-free trajectory $\{\hat{x}^\star(t), \hat{y}^\star(t)\}$ must be the optimal solution of the following problem (P2), otherwise a better solution for problem (P1) can be built based on problem (P2).

$$(\mathrm{P2}): \max_{\{\hat{x}(t),\hat{y}(t)\},E} \quad E \tag{10a}$$

$$\text{s.t.} \int_0^{\hat{T}} \mathcal{F}_{nl}(Q_k(\hat{x}(t),\hat{y}(t)))dt + \bar{E}_k^{\star} \geq E, \forall k \in \mathcal{K}. \tag{10b}$$

$$(\hat{x}(t),\hat{y}(t)) \in \{(x(t_0),y(t_0))|t_0 \in \mathcal{T}\}, \forall t \in [0,\hat{T}]. \tag{10c}$$

Lemma 2. *At the optimal trajectory of problem (P2), the UAV hovers at a number of points, and then flies over them with maximum speed V.*

Proof. The proof is provided in Appendix B. □

According to Lemma 2, trajectory $\{\hat{x}^{\star}(t),\hat{y}^{\star}(t)\}$ is composed of a sequence of hovering points with corresponding hovering durations. Hence, the optimal trajectory $\{x^{\star}(t),y^{\star}(t)\}$ of problem (P1) has an SHF structure, where the UAV successively flies (possibly along a curve) between hovering points with maximum speed V and hovers over each hovering point with the corresponding time duration.

Lemma 3. *For problem (OP), there exists an optimal SHF trajectory with no more than K hovering points (including the starting and ending points).*

Proof. See Appendix C. □

It should be pointed out that as a special case of the 2D scenario, the above lemma also holds for a 1D scenario, which indicates that the maximum number of hovering points proved in [17], i.e., $K+2$, is indeed a loose upper bound and should be updated to K. Moreover, the proved SHF structure also works in a 3D scenario where the devices are distributed in a 3D space. Differently, in 3D scenario, for secure reasons, additional constraints and assumptions are necessary for addressing the safety distance between UAV and GD and possible obstacle blockage when UAV flies very close to GD. Hereby, for facilitation, we only focus on the 2D topology and an example of a UAV trajectory with an SHF structure in a 2D topology is illustrated in Fig. 1. Note that the hovering points may not be exactly above the locations of GDs, as at each time instant different GDs can simultaneously harvest energy due to the broudcasting nature of WPT.

To sum up, for problem (OP) and (P1), there always exists an optimal trajectory satisfying the following two properties: i) the trajectory follows an SHF structure; ii) there are no more than K points, including hovering points, starting point and ending point in the trajectory.

Fig. 1. An example of the SHF structure in a 2D topology with $K = 5$.

IV. Proposed Trajectory Design

In this section, we reformulate the trajectory design problem according to the SHF structure and propose an efficient iterative algorithm for solving the problem. Different from the SHF structure in a 1D topology, the concept of turning points is introduced for a 2D scenario. In particular, a turning point is not a hovering point, but a point at which the UAV changes the flying direction without hovering.

A. Problem Reformulation

We redefine the trajectory (solution) following the SHF structure with at most K hovering points: First, we denote the locations of K possible hovering points, including starting point and ending point, by $(x_i, y_i), i \in \mathcal{K} \triangleq \{1, ..., K\}$ at a height of H. The hovering duration at hovering point i is denoted by t_i and the set of hovering durations is defined as $\mathbf{t} = (t_1, t_2, \cdots, t_K)^T$, $t_i \geq 0, \forall i \in \mathcal{K}$, where $(\cdot)^T$ denotes the operation of transposition. Then, the maximum-speed flight arc between two hovering points (x_i, y_i) and (x_{i+1}, y_{i+1}) is quantized into $N + 1$ line segments by introducing N turning points[1] $(x_{i,j}, y_{i,j}), i \in \mathcal{K}, j = 1, \cdots, N$. In other words, we apply piecewise straight lines with multiple turning points to fit the possible curves between hovering points, as shown in Fig. 2. In particular, as long as the number of turning points is sufficiently large, the approximated curve between two hovering points becomes arbitrarily close to the original one. Hence, the introduction of the turning points does not lose its generality, the approximation will become exact when the number of turning points becomes sufficiently large. In practice, there exists a tradeoff in choosing the number of turning points to balance between complexity and the performance of obtained the trajectory solution.

For simplification, we define $(x_{i,0}, y_{i,0}) = (x_i, y_i)$ and $(x_{i,N+1}, y_{i,N+1}) = (x_{i+1}, y_{i+1})$, $\forall i \in \{1, \cdots, K-1\}$. Hence, the set of hovering points and turning points $(\mathbf{x}, \mathbf{y})$ is given by $\big[(x_{1,0}, x_{1,1}, ..., x_{1,N}, x_{1,N+1}, x_{2,1}, ..., x_{K-1,N+1})^T, (y_{1,0}, y_{1,1}, ..., y_{1,N}, y_{1,N+1}, y_{2,1}, ..., y_{K-1,N+1})^T\big]$. Then, the UAV will successively visit all the points in $(\mathbf{x}, \mathbf{y})$ while hovering at the hovering points and directly flying over turning points. For each line segment from point $(x_{i,j}, y_{i,j})$ to $(x_{i,j+1}, y_{i,j+1})$, the distance $d_{i,j}$ is given by

[1]A similar concept is known as way points [33]–[35]. In general, way points are defined from a UAV flying path perspective, while the turning points here are specifically introduced for the (SHF) trajectory design, i.e., distinguishing with the hovering points.

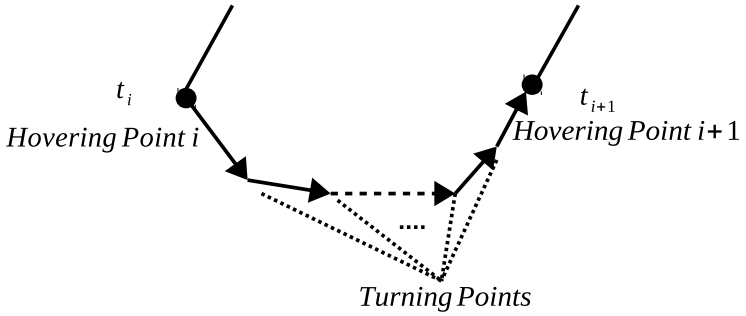

Fig. 2. An example of SHF structure with turning points.

$$d_{i,j} = \sqrt{(x_{i,j+1} - x_{i,j})^2 + (y_{i,j+1} - y_{i,j})^2}. \tag{11}$$

The corresponding trajectory on the straight line segment is denoted by $(\bar{x}_{i,j}(t), \bar{y}_{i,j}(t))$:

$$(\bar{x}_{i,j}(t), \bar{y}_{i,j}(t)) = \left(x_{i,j} + \tfrac{(x_{i,j+1}-x_{i,j})Vt}{d_{i,j}},\ y_{i,j} + \tfrac{(y_{i,j+1}-y_{i,j})Vt}{d_{i,j}}\right), t \in [0, \tfrac{d_{i,j}}{V}]. \tag{12}$$

To sum up, the overall trajectory of UAV within period $\mathcal{T}$ can be formulated as

$$(x(t), y(t)) = \begin{cases} (x_{i'}, y_{i'}), & t \in \left[\sum_{i=1}^{i'-1} t_i + \sum_{i=1}^{i'-1}\sum_{j=0}^{N} \frac{d_{i,j}}{V}, \sum_{i=1}^{i'} t_i + \sum_{i=1}^{i'-1}\sum_{j=0}^{N} \frac{d_{i,j}}{V}\right), 1 \le i' \le K; \\ (\bar{x}_{i',j'}(\delta_{i',j'}(t)), \bar{y}_{i',j'}(\delta_{i',j'}(t))), & t \in \left[\sum_{i=1}^{i'} t_i + \sum_{i=1}^{i'-1}\sum_{j=0}^{N} \frac{d_{i,j}}{V} + \sum_{j=0}^{j'} \frac{d_{i',j}}{V}, \sum_{i=1}^{i'} t_i + \sum_{i=1}^{i'-1}\sum_{j=0}^{N} \frac{d_{i,j}}{V} + \sum_{j=0}^{j'+1} \frac{d_{i',j}}{V}\right), \\ & 1 \le i' < K, 0 \le j' < N; \end{cases} \tag{13}$$

with $\delta_{i',j'}(t) = t - \sum_{i=1}^{i'} t_i - \sum_{i=1}^{i'-1}\sum_{j=0}^{N} \frac{d_{i,j}}{V} - \sum_{j=0}^{j'} \frac{d_{i',j}}{V}$.

Note that there is no benefits if the UAV hovers over a position out of the region (convex hull) of the set of GDs. Therefore, without loss of optimality, we assume that these hovering points and turning points must locate in a rectangular area, i.e., $\min_{k\in\mathcal{K}} w_{x,k} \le \mathbf{x} \le \max_{k\in\mathcal{K}} w_{x,k}$, $\min_{k\in\mathcal{K}} w_{y,k} \le \mathbf{y} \le \max_{k\in\mathcal{K}} w_{y,k}$.

As a result, the energy harvested by GD k during the charging period is given by

$$\begin{aligned} E_k(\mathbf{x}, \mathbf{y}, \mathbf{t}) &= \int_0^T \mathcal{F}_{nl}(Q_k(x(t), y(t)))dt \\ &= \sum_{i=1}^{K} \mathcal{F}_{nl}(Q_k(x_i, y_i))t_i + \sum_{i=1}^{K-1}\sum_{j=0}^{N} \int_0^{\frac{d_{i,j}}{V}} \mathcal{F}_{nl}(Q_k(\bar{x}_{i,j}(t), \bar{y}_{i,j}(t)))dt, \end{aligned} \tag{14}$$

where $\int_0^{\frac{d_{i,j}}{V}} \mathcal{F}_{nl}(Q_k(\bar{x}_{i,j}(t), \bar{y}_{i,j}(t)))dt$ denotes the harvested energy by GD k during the UAV flying from $(x_{i,j}, y_{i,j})$ to $(x_{i,j+1}, y_{i,j+1})$ at the maximum speed V.

With the proposed trajectory structure, problem (P1) can be reformulated to the following (P3).

$$(\mathrm{P3}): \max_{\mathbf{x},\mathbf{y},\mathbf{t},E} \ E \tag{15a}$$

$$s.t.: \ E_k(\mathbf{x},\mathbf{y},\mathbf{t}) \geq E, \forall k \in \mathcal{K}, \tag{15b}$$

$$\sum_{i=1}^{K} t_i + \frac{1}{V}\sum_{i=1}^{K-1}\sum_{j=0}^{N} d_{i,j} \leq T, \tag{15c}$$

$$\min\{\mathbf{w_x}\} \leq \mathbf{x} \leq \max\{\mathbf{w_x}\}, \ \min\{\mathbf{w_y}\} \leq \mathbf{y} \leq \max\{\mathbf{w_y}\}, \tag{15d}$$

$$\mathbf{t} \geq 0, \tag{15e}$$

where the constraint (15c) represents the time constraint such that the whole charging process should be finished within T.

Notice that problem (P3) is non-convex due to the non-convex constraint (15b). And the harvested energy $E_k(\mathbf{x},\mathbf{y},\mathbf{t})$ at k-th GD is built on UAV trajectory $(\mathbf{x},\mathbf{y},\mathbf{t})$ with the assistance of nonlinear implicit function $\mathcal{F}_{nl}$, which makes the related mathematical analysis rather complicated. In the following part, to solve problem (P3), we first introduce a convex approximation for problem (P3) based on the previously introduced convexity property in nonlinear EH process. Subsequently an efficient iterative solution will be proposed by jointly optimizing $\mathbf{t}$ and $(\mathbf{x},\mathbf{y})$ in an iterative manner.

B. Convex Approximation

To obtain a convex approximation of problem (P3), we need to find a convex approximation of the non-convex constraint (15b) in problem (P3). Towards this end, we find a lower-bound concave function $E_k^{(r)}$ such that $E_k \geq E_k^{(r)}$ and the equality holds at a local point $(\mathbf{x}^{(r)},\mathbf{y}^{(r)},\mathbf{t}^{(r)})$.

For the energy E_k harvested by GD k, we provide approximations for the energy harvested during the hovering period, given by $f_{i,k}^{(r)}(\mathbf{x},\mathbf{y},\mathbf{t})$ for each hovering point i, and the energy harvested during flying period, given by $g_{i,j,k}^{(r)}(\mathbf{x},\mathbf{y},\mathbf{t})$ for each flying segment $d_{i,j}$, respectively.

1) Hovering Period: Recall that the function $\mathcal{F}_{nl}(Q_k(x_i,y_i))$ is convex with respect to $(x_i - w_{x,k})^2 + (y_i - w_{y,k})^2$. Then, according the property of convex functions, we have

$$\mathcal{F}_{nl}(Q_k(x_i,y_i))t_i \ \ \geq \ \ -A_{i,k}^{(r)}[(x_i - w_{x,k})^2 + (y_i - w_{y,k})^2]t_i + B_{i,k}^{(r)}t_i, \tag{16}$$

where

$$A_{i,k}^{(r)} = -\left(\mathcal{F}_{nl}(Q_k(x_i^{(r)},y_i^{(r)}))\right)' > 0, \tag{17}$$

$$B_{i,k}^{(r)} = \mathcal{F}_{nl}(Q_k(x_i^{(r)},y_i^{(r)})) + [(x_i^{(r)} - w_{x,k})^2 + (y_i^{(r)} - w_{y,k})^2]A_{i,k}^{(r)}, \tag{18}$$

where $\left(\mathcal{F}_{nl}(Q_k(x_i^{(r)},y_i^{(r)}))\right)'=-\frac{\beta_0 P\mathcal{F}'_{nl}(Q_k(x_i^{(r)},y_i^{(r)}))}{\left((x_i^{(r)}-w_{x,k})^2+(y_i^{(r)}-w_{y,k})^2+H^2\right)^2}$ is the derivative of $\mathcal{F}_{nl}(Q_k(x_i,y_i))$ to $(x_i-w_{x,k})^2+(y_i-w_{y,k})^2$ at point $(x_i^{(r)},y_i^{(r)})$, and $\mathcal{F}'_{nl}(Q_k(x_i^{(r)},y_i^{(r)}))>0$ holds due to the fact that the harvested power $\mathcal{F}_{nl}(Q_k)$ is monotonically increasing in Q_k.

Based on (16), we further have

$$\begin{aligned}
&\mathcal{F}_{nl}(Q_k(x_i,y_i))t_i \ \geq -A_{i,k}^{(r)}[(x_i-w_{x,k})^2+(y_i-w_{y,k})^2]t_i+B_{i,k}^{(r)}t_i\\
=\ & -A_{i,k}^{(r)}\underline{\left((x_i-w_{x,k})^2+(y_i-w_{y,k})^2+C_{i,k}^{(r)}\right)\cdot(t_i+D_{i,k}^{(r)})}+A_{i,k}^{(r)}C_{i,k}^{(r)}t_i+B_{i,k}^{(r)}t_i\\
&+A_{i,k}^{(r)}D_{i,k}^{(r)}[(x_i-w_{x,k})^2+(y_i-w_{y,k})^2] \qquad (19a)\\
\geq\ & -A_{i,k}^{(r)}\cdot\underline{\frac{1}{2}\left((x_i-w_{x,k})^2+(y_i-w_{y,k})^2+C_{i,k}^{(r)}\right)^2}-A_{i,k}^{(r)}\cdot\underline{\frac{1}{2}(t_i+D_{i,k}^{(r)})^2}+A_{i,k}^{(r)}C_{i,k}^{(r)}t_i+B_{i,k}^{(r)}t_i\\
&+A_{i,k}^{(r)}D_{i,k}^{(r)}[(x_i-w_{x,k})^2+(y_i-w_{y,k})^2], \qquad (19b)
\end{aligned}$$

where the approximation from (19a) to (19b) results from the inequality of arithmetic and geometric means, i.e., the inequality $ab\leq\frac{1}{2}a^2+\frac{1}{2}b^2$ holds $\forall a,b\in\mathcal{R}^+$ and the equality holds when $a=b$. And the non-negative constants $C_{i,k}^{(r)}$ and $D_{i,k}^{(r)}$ are defined as

$$C_{i,k}^{(r)}=\max\{t_i^{(r)}-(x_i^{(r)}-w_{x,k})^2-(y_i^{(r)}-w_{y,k})^2,0\}, \qquad (20)$$

$$D_{i,k}^{(r)}=(x_i^{(r)}-w_{x,k})^2+(y_i^{(r)}-w_{y,k})^2+C_{i,k}^{(r)}-t_i^{(r)}. \qquad (21)$$

In addition, the function $(x_i-w_{x,k})^2+(y_i-w_{y,k})^2$ is convex in x_i and y_i. Hence, we have

$$\begin{aligned}
&\mathcal{F}_{nl}(Q_k(x_i,y_i))t_i\\
\geq\ & -\frac{1}{2}A_{i,k}^{(r)}((x_i-w_{x,k})^2+(y_i-w_{y,k})^2+C_{i,k}^{(r)})^2-\frac{1}{2}A_{i,k}^{(r)}(t_i+D_{i,k}^{(r)})^2+A_{i,k}^{(r)}C_{i,k}^{(r)}t_i+B_{i,k}^{(r)}t_i\\
&+A_{i,k}^{(r)}D_{i,k}^{(r)}[(x_i^{(r)}-w_{x,k})(2x_i-x_i^{(r)}-w_{x,k})+(y_i^{(r)}-w_{y,k})(2y_i-y_i^{(r)}-w_{y,k})]\\
\triangleq\ & f_{i,k}^{(r)}(\mathbf{x},\mathbf{y},\mathbf{t}). \qquad (22)
\end{aligned}$$

As a polynomial, the concavity of $f_{i,k}^{(r)}(\mathbf{x},\mathbf{y},\mathbf{t})$ in $(\mathbf{x},\mathbf{y},\mathbf{t})$ can be easily shown.

2) Maximum-Speed Flying Period: For each flying segment, the expression of the harvested energy contains an integral over the segment, which motivates us to perform a differentiation approach for the convex approximation.

We first uniformly divide each segment of flying path into L subsegments, where L is sufficiently large enough to keep the subsegments small enough, so that in each subsegment the UAV can be assumed to be static, i.e., a subsegment is indeed a static UAV position with a virtual hovering duration. For each straight segment $(x_{i,j},y_{i,j})\rightarrow(x_{i,j+1},y_{i,j+1})$, the trajectory $(\bar{x}_{i,j}(t),\bar{y}_{x,y}(t))$ is equivalently (when L is sufficiently large) split into L subsegments (static UAV

positions): $\bar{x}_{i,j,l} = x_{i,j} + l/L(x_{i,j+1} - x_{i,j})$, $\bar{y}_{i,j,l} = y_{i,j} + l/L(y_{i,j+1} - y_{i,j})$, $\forall l \in \{0, 1, ..., L-1\}$. Recall that $d_{i,j}$ is the segment length, given in (11). Then, the virtual hovering duration at each subsegment is $\frac{d_{i,j}}{LV}$. The energy harvested at device k during UAV flying in segment $(x_{i,j}, y_{i,j}) \to (x_{i,j+1}, y_{i,j+1})$ is denoted by:

$$\int_0^{\frac{d_{i,j}}{V}} \mathcal{F}_{nl}(Q_k(\bar{x}_{i,j}(t), \bar{y}_{i,j}(t)))dt = \lim_{L\to\infty} \sum_{l=0}^{L-1} \mathcal{F}_{nl}(Q_k(\bar{x}_{i,j,l}, \bar{y}_{i,j,l}) \cdot \frac{d_{i,j}}{LV}, \tag{23}$$

where $\bar{x}_{i,j,l}$, $\bar{y}_{i,j,l}$ and $d_{i,j}$ are all functions with variables $x_{i,j}$, $y_{i,j}$, $x_{i,j+1}$ and $y_{i,j+1}$.

Remark. *Note that quantizing a flying segment into L virtual static positions does not introduce any further variables, as the locations of these positions are constant for a given L, i,e. being uniformly located on the segment. Moreover, Eq.* (23) *confirms that as L approaches to infinity, the error of the quantization vanishes.*

Next, an approximation is going to be performed for each subsegment. In this way, we can finally obtain a concave approximation of the integral charged energy on each straight segment, by approaching the sufficient large value L to infinity.

According to the convex property of the linear process $\mathcal{F}_{nl}$, which is applied during the approximation of hovering period, we have

$$\begin{aligned}
&\int_0^{\frac{d_{i,j}}{V}} \mathcal{F}_{nl}(Q_k(\bar{x}_{i,j}(t), \bar{y}_{i,j}(t)))dt \\
\geq\ & \lim_{L\to\infty} \sum_{l=0}^{L-1} \left[-A^{(r)}_{i,j,k,l}((\bar{x}_{i,j,l} - w_{x,k})^2 + (\bar{y}_{i,j,l} - w_{y,k})^2) + B^{(r)}_{i,j,k,l} \right] \cdot \frac{d_{i,j}}{LV} \\
=\ & \left(G^{(r)}_{i,j,k} - h^{(r)}_{i,j,k}(\mathbf{x}, \mathbf{y}, \mathbf{t}) \right) \cdot d_{i,j},
\end{aligned} \tag{24}$$

where

$$A^{(r)}_{i,j,k,l} = -\left(\mathcal{F}_{nl}(Q_k(\bar{x}^{(r)}_{i,j,l}, \bar{y}^{(r)}_{i,j,l})) \right)' > 0, \tag{25}$$

$$B^{(r)}_{i,j,k,l} = \mathcal{F}_{nl}(Q_k(\bar{x}^{(r)}_{i,j,l}, \bar{y}^{(r)}_{i,j,l})) + \left((\bar{x}^{(r)}_{i,j,l} - w_{x,k})^2 + (\bar{y}^{(r)}_{i,j,l} - w_{y,k})^2 \right) A^{(r)}_{i,j,k,l}, \tag{26}$$

$$h^{(r)}_{i,j,k}(\mathbf{x}, \mathbf{y}, \mathbf{t}) = \lim_{L\to\infty} \sum_{l=0}^{L-1} \frac{1}{LV} A^{(r)}_{i,j,k,l} \left((\bar{x}_{i,j,l} - w_{x,k})^2 + (\bar{y}_{i,j,l} - w_{y,k})^2 + H^2 \right), \tag{27}$$

$$G^{(r)}_{i,j,k} = \lim_{L\to\infty} \sum_{l=0}^{L-1} \frac{1}{LV} B^{(r)}_{i,j,k,l}. \tag{28}$$

Note that $h^{(r)}_{i,j,k}(\mathbf{x}, \mathbf{y}, \mathbf{t})$ is a positive convex function and $G^{(r)}_{i,j,k}$ is a positive value. It is worth

to mention that although function $h_{i,j,k}^{(r)}(\mathbf{x},\mathbf{y},\mathbf{t})$ is defined as an accumulation of infinite convex functions, as L tends to infinity, $h_{i,j,k}^{(r)}(\mathbf{x},\mathbf{y},\mathbf{t})$ can be equivalently reconstructed as a polynomial function $h_{i,j,k}^{(r)}(x_{i,j},x_{i,j+1},y_{i,j},y_{i,j+1})$, in which the coefficients are obtained from integrals. In particular, as both $A_{i,j,k,l}^{(r)}$ and $B_{i,j,k,l}^{(r)}$ are obtained based on l/L, by defining a variable $z = l/L \in [0,1]$, we can build

$$A_{i,j,k}^{(r)}(z) \triangleq A_{i,j,k,l}^{(r)}\Big|_{\frac{l}{L}=z},\ B_{i,j,k}^{(r)}(z) \triangleq B_{i,j,k,l}^{(r)}\Big|_{\frac{l}{L}=z}, \tag{29}$$

$$\bar{x}'_{i,j}(z) \triangleq x_{i,j,l}\Big|_{\frac{l}{L}=z} = x_{i,j} + z(x_{i,j+1}-x_{i,j}),\ \bar{y}'_{i,j}(z) \triangleq y_{i,j,l}\Big|_{\frac{l}{L}=z} = y_{i,j} + z(y_{i,j+1}-y_{i,j}). \tag{30}$$

And the factor $1/L$ can be directly considered as the differentiation of variable z. Then, we have

$$h_{i,j,k}^{(r)}(\mathbf{x},\mathbf{y},\mathbf{t}) = \int_0^1 \frac{1}{V} A_{i,j,k}^{(r)}(z)\left((\bar{x}'_{i,j}(z)-w_{x,k})^2 + (\bar{y}'_{i,j}(z)-w_{y,k})^2 + H^2\right) dz, \tag{31}$$

$$G_{i,j,k}^{(r)} = \int_0^1 \frac{1}{V} B_{i,j,k}^{(r)}(z) dz. \tag{32}$$

Remark. *Combining* (31) *and* (32) *to the approximation in* (24)*, the two sides of the approximation are actually an integral and the difference of two weighted integrals. This confirms that the introduction of variable L is only for facilitating the derivations for the approximation and that the approximated results are not influenced by L.*

As the segment length $d_{i,j}$ is a function of $(\mathbf{x},\mathbf{y})$, i.e., $d_{i,j} = d_{i,j}(\mathbf{x},\mathbf{y})$, a further approach for approximation is still required. According to the inequality of arithmetic and geometric means, $\forall a,b \in \mathcal{R}^+$ and $F > 0$, $ab = \frac{1}{F}Fab \le \frac{1}{F}(\frac{1}{2}F^2a^2 + \frac{1}{2}b^2)$ holds, while the equality holds when $Fa = b$. Then, for $F_{i,j,k}^{(r)} = \frac{d_{i,j}^{(r)}}{h_{i,j,k}^{(r)}(\mathbf{x}^{(r)},\mathbf{y}^{(r)},\mathbf{t}^{(r)})}$, we have

$$\int_0^{\frac{d_{i,j}}{V}} \mathcal{F}_{nl}(Q_k(\bar{x}_{i,j}(t),\bar{y}_{i,j}(t)))dt \ge -\frac{F_{i,j,k}^{(r)}}{2}\left(h_{i,j,k}^{(r)}(\mathbf{x},\mathbf{y},\mathbf{t})\right)^2 - \frac{1}{2F_{i,j,k}^{(r)}}d_{i,j}^2 + G_{i,j,k}^{(r)}d_{i,j}.$$

Note that $d_{i,j}^{(r)} = \sqrt{(x_{i,j+1}^{(r)}-x_{i,j}^{(r)})^2 + (y_{i,j+1}^{(r)}-y_{i,j}^{(r)})^2} > 0$ holds and keeps $F_{i,j,k}^{(r)} > 0$, otherwise the points $(x_{i,j}^{(r)}, y_{i,j}^{(r)})$ and $(x_{i,j+1}^{(r)}, y_{i,j+1}^{(r)})$ are the same point and can be merged into a single point.

As $d_{i,j} = d_{i,j}(\mathbf{x},\mathbf{y})$ is a convex function, we have

$$\begin{aligned}
&\int_0^{\frac{d_{i,j}}{V}} \mathcal{F}_{nl}(Q_k(\bar{x}_{i,j}(t),\bar{y}_{i,j}(t)))dt \\
&\ge -\frac{F_{i,j,k}^{(r)}}{2}\left(h_{i,j,k}^{(r)}(\mathbf{x},\mathbf{y},\mathbf{t})\right)^2 - \frac{d_{i,j}^2}{2F_{i,j,k}^{(r)}} + \frac{G_{i,j,k}^{(r)}}{d_{i,j}^{(r)}}\left[(x_{i,j+1}^{(r)}-x_{i,j}^{(r)})(x_{i,j+1}-x_{i,j}) + (y_{i,j+1}^{(r)}-y_{i,j}^{(r)})(y_{i,j+1}-y_{i,j})\right] \\
&\triangleq g_{i,j,k}^{(r)}(\mathbf{x},\mathbf{y},\mathbf{t}).
\end{aligned} \tag{33}$$

As $\left(h_{i,j,k}^{(r)}(\mathbf{x},\mathbf{y},\mathbf{t})\right)^2$ and $d_{i,j}^2$ are both convex in $(\mathbf{x},\mathbf{y},\mathbf{t})$, $g_{i,j,k}^{(r)}(\mathbf{x},\mathbf{y},\mathbf{t})$ is concave in $(\mathbf{x},\mathbf{y},\mathbf{t})$.

According to the above approximations for the hovering and flying periods, given a point $(\mathbf{x}^{(r)},\mathbf{y}^{(r)},\mathbf{t}^{(r)})$, for a random feasible point $(\mathbf{x},\mathbf{y},\mathbf{t})$ of problem (P3), it holds

$$E_k(\mathbf{x},\mathbf{y},\mathbf{t}) \geq \sum_{i=1}^{K} f_{i,k}^{(r)}(\mathbf{x},\mathbf{y},\mathbf{t}) + \sum_{i=1}^{K-1}\sum_{j=0}^{N} g_{i,j,k}^{(r)}(\mathbf{x},\mathbf{y},\mathbf{t}) = E_k^{(r)}(\mathbf{x},\mathbf{y},\mathbf{t}). \tag{34}$$

Note that $E_k^{(r)}(\mathbf{x},\mathbf{y},\mathbf{t})$ is a concave function and the equality in (34) holds at the local point $(\mathbf{x}^{(r)},\mathbf{y}^{(r)},\mathbf{t}^{(r)})$.

In the next subsection, we propose an iterative solution utilizing the above convex approximation of the constraint.

C. Proposed Iterative Solution

For the iterative solution, we start with an initialized feasible local point $(\mathbf{x}^{(0)},\mathbf{y}^{(0)},\mathbf{t}^{(0)})$. The iteration counter is set to be 0, i.e., $r=0$. After initialization, in the r-th iteration, we build a concave approximation of harvested energy at each device over the local point $(\mathbf{x}^{(r)},\mathbf{y}^{(r)},\mathbf{t}^{(r)})$, according to (34). By replacing the harvested energy in (P3) as its approximation, we have problem (P4):

$$\begin{aligned}
(\mathrm{P4}): \max_{\mathbf{x},\mathbf{y},\mathbf{t},E} \quad & E && \text{(35a)}\\
s.t.: \quad & E_k^{(r)}(\mathbf{x},\mathbf{y},\mathbf{t}) \geq E, \forall k \in \mathcal{K}, && \text{(35b)}\\
& \text{(15c), (15d), (15e).}
\end{aligned}$$

Clearly, the introduction of the concave approximation $E_k^{(r)}(\mathbf{x},\mathbf{y},\mathbf{t})$ transforms constraint (15b) into a convex one (35b). Therefore, problem (P4) is convex, i.e., can be solved efficiently via various optimization techniques. In this work, we use a sub-gradient method, i.e. the ellipsoid method with constraints [36], to solve problem (P4).

The solution of problem (P4) is used as the local point in the next iteration. Note that the following relation holds for the objective values between two adjacent iterations:

$$\begin{aligned}
& \min_k \left\{E_k(\mathbf{x}^{(r)},\mathbf{y}^{(r)},\mathbf{t}^{(r)})\right\} = \min_k \left\{E_k^{(r)}(\mathbf{x}^{(r)},\mathbf{y}^{(r)},\mathbf{t}^{(r)})\right\}\\
\leq\ & \min_k \left\{E_k^{(r)}(\mathbf{x}^{(r+1)},\mathbf{y}^{(r+1)},\mathbf{t}^{(r+1)})\right\} \leq \min_k \left\{E_k(\mathbf{x}^{(r+1)},\mathbf{y}^{(r+1)},\mathbf{t}^{(r+1)})\right\}.
\end{aligned} \tag{36}$$

In other words, the objective function constantly increases after each iteration. Hence, the algorithm will eventually lead to a converged solution.

Algorithm 1 : Iterative Algorithm.

Initialization

Initialize $(\mathbf{x}^{(0)}, \mathbf{y}^{(0)}, \mathbf{t}^{(0)})$ based on salesman and set $r = 0$.

Iteration

a) Build approximation $E_k^{(r)}(\mathbf{x}, \mathbf{y}, \mathbf{t})$ on point $(\mathbf{x}^{(r)}, \mathbf{y}^{(r)}, \mathbf{t}^{(r)})$;

b) Solve the convex problem (P4),obtain optimal $E^\star$ and optimal point $(\mathbf{x}^\star, \mathbf{y}^\star, \mathbf{t}^\star)$;

c) **If** improvement of $E^\star$ compared with previous iteration is below ϵ

stop iteration;

Else

$(\mathbf{x}^{(r+1)}, \mathbf{y}^{(r+1)}, \mathbf{t}^{(r+1)}) = (\mathbf{x}^\star, \mathbf{y}^\star, \mathbf{t}^\star)$;

$r = r + 1$;

go back to **a).**

D. Trajectory Initialization

For the initialization process, we introduce an efficient initial trajectory which is already introduced in [16]. The path of trajectory is initialized as the shortest path which connects all GDs together and passes through each device only once, which can be found based on the solution of Travelling Salesman Problem [37]. Then, on the shortest path, we uniformly scatter K hovering points and uniformly scatter N turning points between each two neighbour hovering points to form an initial path $(\mathbf{x}^{(0)}, \mathbf{y}^{(0)})$.

If the minimum flying time on the initial path is less than the whole charging duration T, i.e., $T - \frac{1}{V}\sum_{i=1}^{K-1}\sum_{j=0}^{N} d_{i,j}^{(0)} \geq 0$, we uniformly allocate the remaining charging time on these hovering points, i.e., $\mathbf{t}^{(0)} = \frac{T - \frac{1}{V}\sum_{i=1}^{K-1}\sum_{j=0}^{N} d_{i,j}^{(0)}}{K} \cdot (1, ..., 1)^T$. After that, we develop an initial trajectory in which the UAV flies between hovering positions with maximum UAV speed V. When the charging duration is not sufficient to cover the initial path $(\mathbf{x}^{(0)}, \mathbf{y}^{(0)})$, we apply a trajectory scaling mentioned in [16] based on an optimal single hovering point $(x^\star, y^\star)$ which maximizes the function $\min_{k \in \mathcal{K}} \{\mathcal{F}_{nl}(\frac{\beta_0 P}{(x - w_{x,k})^2 + (y - w_{y,k})^2 + H^2})\}$. It is clear that the optimal point $(x^\star, y^\star)$ can be searched out in the operation area. Based on the optimal single hovering point $(x^\star, y^\star)$, the original path $(\mathbf{x}^{(0)}, \mathbf{y}^{(0)})$ is modified as: $(\mathbf{x}^{(0)}, \mathbf{y}^{(0)})^{\text{new}} = (\mathbf{x}^{(0)}, \mathbf{y}^{(0)}) + (1 - \kappa)\left((x^\star, y^\star) - (\mathbf{x}^{(0)}, \mathbf{y}^{(0)})\right)$, where $\kappa = \frac{VT}{\sum_{i=1}^{K-1}\sum_{j=0}^{N} d_{i,j}^{(0)}} < 1$ is the linear scaling factor. After modification, in the initial trajectory, the UAV still flies between hovering positions with maximum UAV speed V.

After all, according to the above analysis, the flow of this iterative solution is described in Algorithm 1.

E. Complexity Analysis

Following the complexity analysis approach in [17], we study the complexity of our proposed algorithm based on the ellipsoid method, which is a stable solution tool for convex problems and can facilitate the complexity analysis [38]. While solving a convex problem, the ellipsoid method generates a sequence of ellipsoids and those ellipsoids will eventually converge to the optimal. According to [38], in each call of ellipsoid update, the computational complexity mainly results from the update of the ellipsoid matrix and the corresponding calculations on the objective function and constraints on the centre point of the ellipsoid. In each iteration of our proposed algorithm, a single convex problem with in total $2NK + 3K - 2N$ variables is solved, which results in $\mathcal{O}((2NK+3K-2N)^2 \log(\frac{1}{\xi}))$ calls for ellipsoid updates where ξ denotes the convergence threshold for ellipsoids. For each call of ellipsoid update, the update of ellipsoid matrix contributes to a complexity of $\mathcal{O}((2NK + 3K - 2N)^2)$ and additional calculation in constraints costs a complexity of $\mathcal{O}((2NK+3K-2N)K)$. Denoting the number of iterations of the algorithm till convergence by φ, the total complexity level of proposed algorithm can be expressed as

$$\begin{aligned}&\mathcal{O}\left(\varphi(2NK + 3K - 2N)^2 \log(\frac{1}{\xi})\right) \cdot \left(\mathcal{O}((2NK + 3K - 2N)^2) + \mathcal{O}((2NK + 3K - 2N)K)\right)\\ &= \mathcal{O}\left(\varphi(2NK + 3K - 2N)^4 \log(\frac{1}{\xi})\right). \end{aligned} \tag{37}$$

Obviously, the complexity will increase significantly in the number of GDs K and the number of turning points N.

V. Performance Evaluation

In this section, the proposed iterative algorithm is numerically evaluated in terms of the minimal average harvested power among GDs. We consider a square charging area with a width of 30m. The GDs are randomly located in the charging area. Unless otherwise stated, the simulation parameters are set as: $K = 5$, $N = 1$, $\beta_0 = -30$dB, $H = 5$m, $P = 40$dBm and $T = 40$s. The results are averaged over 40 different random typologies. Moreover, in order to evaluate the performance of the proposed algorithm, we compare the results to the following benchmarks:

- Upper bound: the upper bound of each topology is obtained by ignoring the maximum flying speed in the constraints. It represents the optimal performance when the UAV speed limit is ignored. Hence, a small performance gap between a trajectory design (with UVA

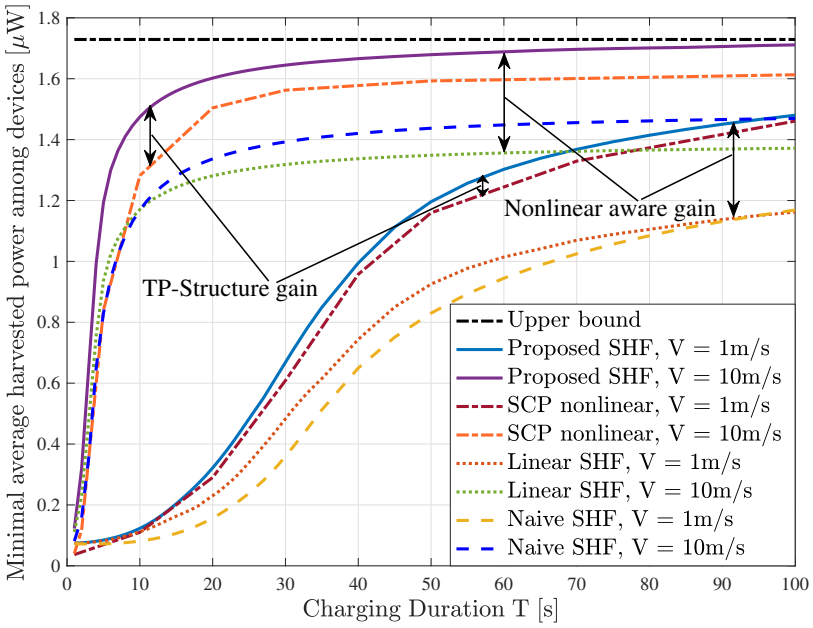

Fig. 3. Average performance comparison with varying charging duration T.

speed limits) and this upper bound, especially when the UAV flying speed is increased, indicates a high efficiency of the design, and vice versa.

- Linear SHF with turning points: this scheme optimizes the minimal harvested power among devices considering an inaccurate linear property of the charging process. It can be easily achieved via the same procedure as our proposed strategy. Then, the average harvested power is calculated based on the obtained trajectory and an accurate nonlinear EH process. The performance gap between this scheme and the proposed design illustrates the performance improvement by considering nonlinear EH in the design.
- Nonlinear successive convex programming (SCP) based on SHF: in order to show the performance advantage of introducing the turning points to the SHF trajectory design, the SCP-based solution is also provided as a benchmark. As a popular strategy in trajectory design, SCP method approximates a trajectory into a large number of points according to a time resolution, and optimizes the trajectory by optimizing the positions of these points. In this scheme, we directly apply SCP based on nonlinear model and an initialized SHF-structured trajectory, and then evaluate the trajectory by assuming UAV flying between each two points with a constant speed.
- Naive SHF: this scheme is actually the initial trajectory we introduced in the initialization step in Section IV-D, which gives a most intuitive trajectory design.

We start with Fig. 3 to depict the minimal averaged harvested power of the proposed design and

different benchmarks under a wide range of charging duration. It is observed that the proposed design outperforms the Linear SHF and Naive SHF as well as the nonlinear SCP based on SHF in all ranges of the charging duration, no matter the UAV speed limit is strict or loose. In particular, a significant performance gain due to applying the non-linear EH process is illustrated, when comparing the proposed SHF with the linear SHF. This gain indicates the advantage of the proposed trajectory design and confirms the necessity of the work. Moreover, under the maximum speed constraint of $10m/s$, the result of proposed SHF gradually converges to the upper bound (as the total charging duration increases), while the results of Linear SHF (with turning points) and Naive SHF converge to a saturation point which is far lower. Furthermore, it is also observed that with a high maximum speed and a long charging duration, even the Naive SHF has a better performance than the Linear SHF. Please note that the Naive SHF scheme is a very simple algorithm with much lower computational complexity compared with Linear SHF. This result indicates again that ignoring this non-linearity results in a significant performance loss in the design of practical WPT systems, which possibly makes the design worse than a naive one. By comparing the proposed design with the nonlinear SCP based on SHF, we observe a performance gain from turning point (TP)-based SHF structure, which confirms the advantages of introduced trajectory structure with turning points. As resulted trajectory of SCP does not follow an SHF structure, the performance is largely limited by the resolution (we set the time resolution of SCP to $0.5s$ in the simulation). On the other hand, by letting the time resolution go to zero, the solution of SCP approaches to an SHF trajectory with infinite turning points. Hence, both the nonlinear SCP and the proposed SHF with turning points are promising ways to approach to the optimal trajectory solution, but the complexity costs are significantly different as the proposed SHF has already shown an about 30 times higher efficiency than the nonlinear SCP during simulations to obtain the result in Fig. 3. A detailed discussion of the complexity can be found in our previous work [17], which indicates the significant drawback of SCP in computational complexity.

In addition, in order to provide more insights of behaviours of the proposed design, a set of trajectory solutions of the proposed design and the other benchmarks are compared in Fig. 4. Four groups of results conducted under the scenarios with the same network (same GDs) topology but different maximum UAV speeds are provided in four sub-figures. It can be found that with a low maximum speed, e.g., $V = 1$m/s in Fig. 4(a) and $V = 2$m/s in Fig. 4(b), the trajectory of Naive SHF is obtained by scaling the path connecting the devices' locations. This "naive" trajectory

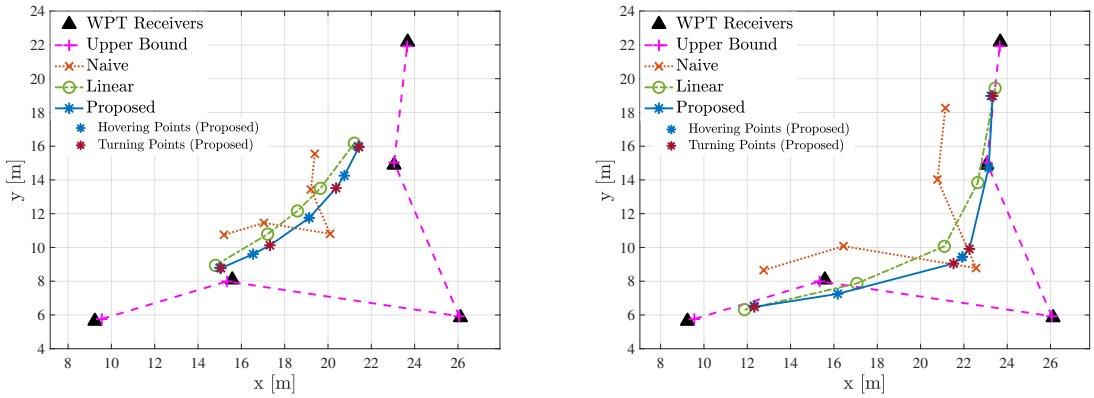

(a) $T = 10$s, $V = 1$m/s (b) $T = 10$s, $V = 2$m/s

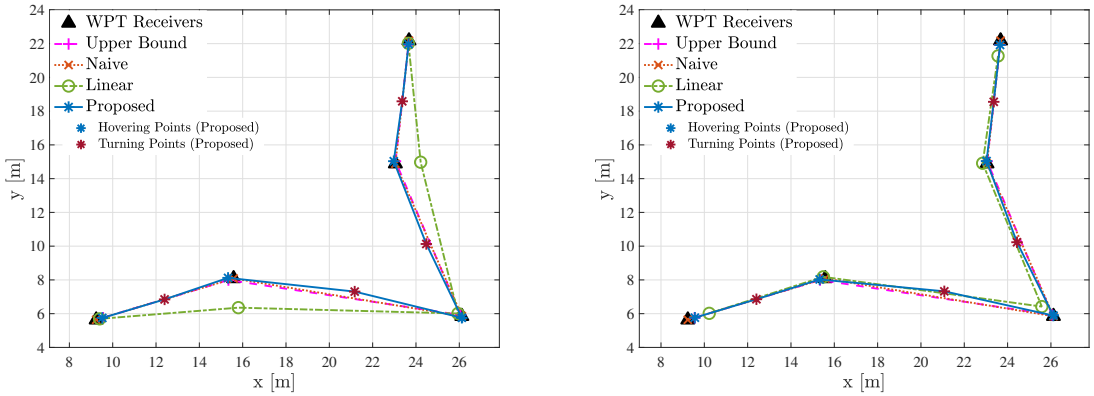

(c) $T = 10$s, $V = 5$m/s (d) $T = 10$s, $V = 10$m/s

Fig. 4. Trajectory examples of the proposed design in comparison to other benchmarks. The number of turning points in this simulation is set to $N = 1$. We acknowledge that letting $N = 1$ is not able to make the designed trajectory smooth, this choice is limited by the fact that setting a higher value of N makes the trajectories become more difficult to be distinguished. On the other hand, the WPT performance and algorithm complexity with different number turning points are specifically studied in Fig. 9, where the results indicate that the WPT performance of the proposed design with a small N is already competitive.

is quite different from trajectories of the proposed SHF and the Linear SHF, and makes the performance of the Naive SHF be the worst one when both the maximum UAV speed charging duration are quite limited, as shown in Fig. 3. In addition, when the UAV is allowed to fly with a relatively high speed, as shown in Fig. 4(c) and Fig. 4(d), both trajectories of the upper bound case and the proposed design suggest having hovering points to be close to the devices' locations. At the same time, the trajectories of the Linear SHF do not follow this suggestion, which makes its performance be the worst one among all schemes. It can be concluded from the results that in comparison to the design ignoring the non-linear EH, the non-linearity generally makes the designed trajectory get closer to the locations of the GDs. It should be pointed out that although the designed trajectories look similar at the first glance when the UAV speed limit is large, the differences in hovering points and different allocated hovering duration actually result in a significant performance gap in terms of the harvested DC energy, as displayed in Fig. 3.

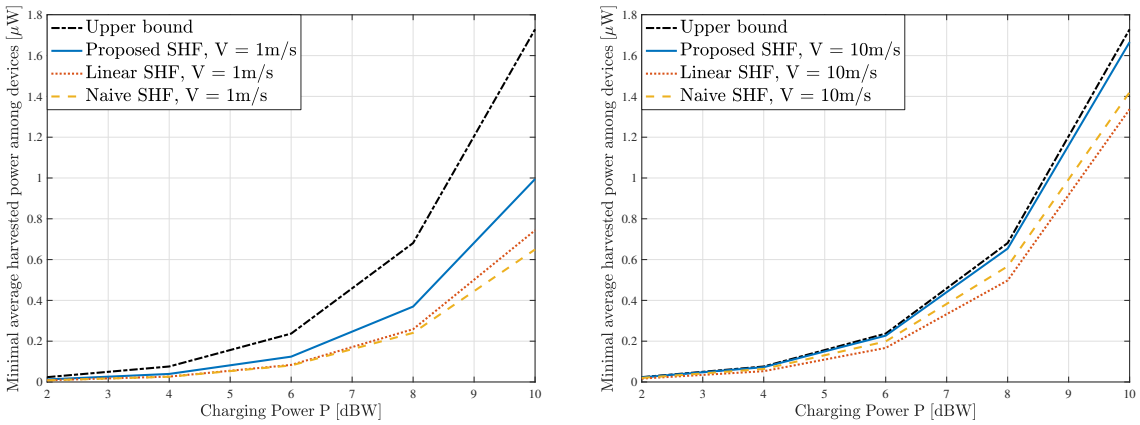

(a) $T = 40$s, $V = 1$m/s (b) $T = 40$s, $V = 10$m/s

Fig. 5. Average performance comparison with varying charging power P.

Moreover, we study the average WPT performance of the proposed design over 40 different network topologies. The influence of UAV's transmit power on the minimal average harvested power among GDs is shown in Fig. 5. Clearly, the performance gap between the proposed design and the upper bound is not constant. This is due to the fact that the upper bound case ignores the UAV speed limit, i.e., the UAV could jump from one hovering point to the next, while in other schemes it costs time to fly via the path (with infinity location points) having a poor WPT performance than hovering points. This makes this upper bound not tight for the case with a strict UAV speed constraint. This is also the reason why it can be only treated as a benchmark performance bound but not the objective of the design. In particular, as shown in Fig. 5(a) with $V = 1$m/s, this gap is is getting larger as transmit power increases. However, from the results shown in Fig. 5(b), when the maximum UAV speed is high, e.g., $V = 10$m/s, this gap becomes tiny. In comparison to the linear SHF and naive SHF, we observe again the performance advantage of the proposed design. In particular, this performance advantage is more significant when the transmit power is high.

Next, the influence of the number of GDs on the minimal average harvested power is investigated. The results are provided in Fig. 6. The results at each number of GDs are also averaged over 40 different devices topologies in the following way. We start with $K = 3$ and randomly generate the locations of 3 devices in 40 topologies. We obtain the average WPT performance of all schemes at $K = 3$ and save the topologies. Then, for $K = 4$ we used the saved topologies and additionally randomly drop the fourth device in each topology. We do the same process for

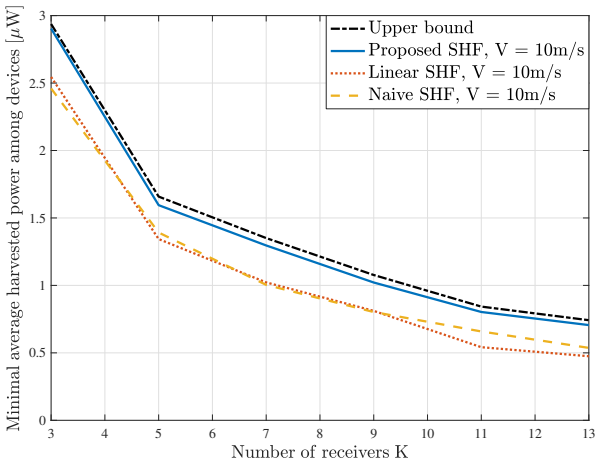

Fig. 6. Average performance comparison with varying number of GDs K.

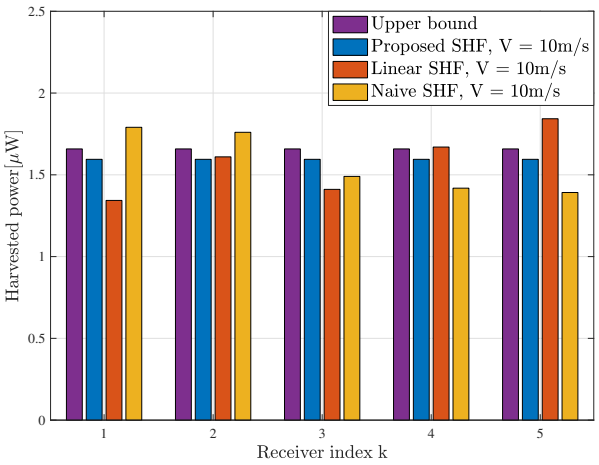

Fig. 7. An example on harvested power of each GD. In the simulation, we set $T = 40$s and $V = 10$m/s.

the rest of devices. In this way, we can get rid of the impact of device density randomness[2] and observe the true performance behavior of the schemes versus the number of GDs. From the figure, we learn that the WPT performance is decreasing in the number of devices. This is due to the fact that as more devices are deployed in the network, an efficient trajectory for fewer devices are high likely not able to cover the requirement of the new device. Since the objective is to maximize the worst harvested power among all GDs, the WPT performance of all schemes is thus degraded. On the other hand, the performance of our proposed SHF scheme is close to the upper bound within all range of the number of devices, which indicates that the performance advantage of our design is not influenced by the number of GDs needs the served.

Furthermore, we compare the proposed design in comparison to benchmarks with respect to the harvested power of at each device. The results are conducted under a fixed (obtained randomly) network topology with 5 devices. As shown in in Fig. 7, the WPT performance of all devices are all almost equal to each other under the upper bound case and the proposed design. Since the aim is to maximize the worst performance among all devices, this observation confirms the efficiency of our design. Meanwhile, the Naive SHF scheme does not consider fairness among devices, which results in a low WPT performance (minimal harvested power among devices). In addition, although the linear SHF scheme takes the fairness into account, due to the inaccuracy of the linear EH model, the scheme has a even lower WPT performance than the naive one. In addition, we also checked the corresponding trajectories (not shown here), it confirms with

[2]Note that a poor topology with 2 far apart devices has a significantly lower performance than a topology with 10 devices closing to each other.

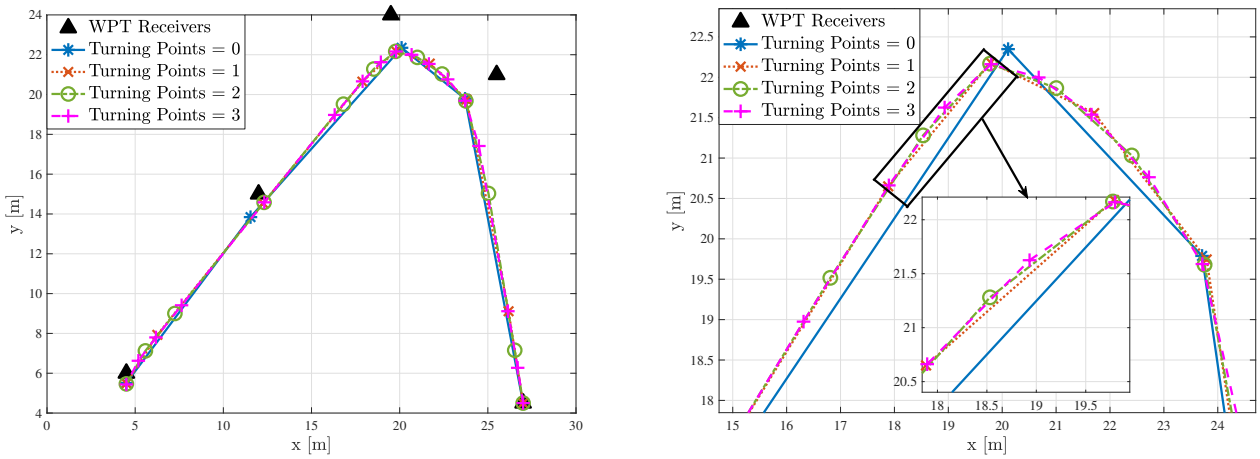

(a) Full trajectories (b) Local enlargement

Fig. 8. Trajectories with various number of turning points under a given topology of GDs. In the simulation we set $T = 15$s, $V = 3$m/s.

Fig. 4(d) that when T and V are relatively large, the UAV flying paths (including hovering points) of different schemes look quite similar. However, the corresponding hovering durations are different, which makes the upper bound case and the proposed design outperform the other two schemes.

Finally, we investigate the impact of the number of turning points in the proposed trajectory design. First in Fig. 8, the trajectories (obtained via the proposed design) with different number of turning points are depicted. It is shown that having more turning points makes the path smoother at the corner part of the trajectory curve, which is especially shown in Fig. 8(b) as a local enlargement. On the other hand, when the number of turning points is larger than one, the change on the path is not obvious by increasing the turning points. This observation is also reflected in terms of the minimal harvested power in Fig. 9, where the impact of turning

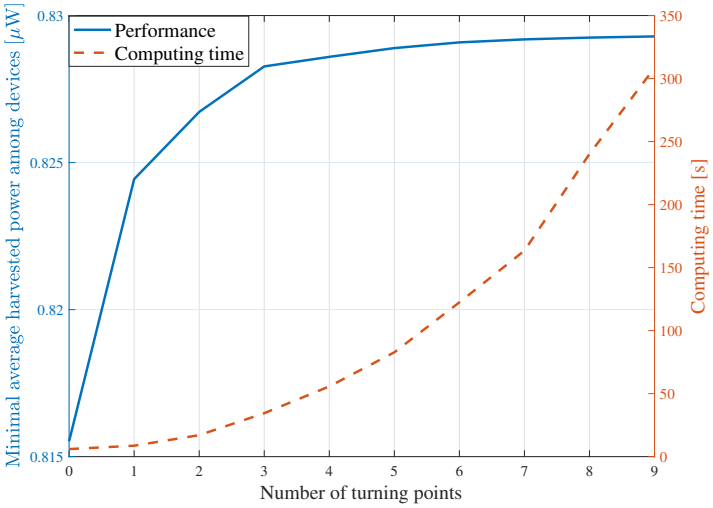

Fig. 9. Impact of turning points on the performance and computing time.

points on the performance and the computing time is investigated. From Fig. 9, it is learnt that with a increasing number of turning points the improvement of the WPT performance becomes slow and finally saturates. On the other hand, Fig. 9 also shows that the computing time is exponentially increasing in the number of turning points. This confirms that the turning points do introduce a trade-off between the WPT performance and the complexity to the network design. Combining the results in Fig. 8 and Fig. 9, a relatively small number of turning points (e.g., 3,4,5) is suggested, as it achieves a competitive WPT performance while costs a relatively lower complexity.

VI. Concluding Remarks

In this paper, we focused on a UAV-assisted WPT network while considering the nonlinear EH process. With a maximum speed limit of UAV, we studied a UAV trajectory design problem aiming at maximizing of the minimum harvested energy among GDs. We firstly characterized the structure of an optimal UAV trajectory in a 2D topology where GDs are deployed in an area. Based on the characterization, we established the optimal trajectory structure – SHF structure, and further introduced turning points in order to approximate the possible curves between hovering points. With the modified optimal trajectory structure, the original problem with infinite variables is transformed to one with finite variables. By introducing turning points, the SHF structure becomes more flexible to be implemented in optimization problems and extended into more scenarios. Secondly, with the help of the convexity property in the nonlinear EH model, we introduce a convex approximation of the problem following the SHF structure with turning points, and subsequently proposed an iterative algorithm for the UAV trajectory design.

Via simulations, we found that the performance of our proposed design approaches to the upper bound, especially when the charging duration or maximum speed limit increases, which indicates the efficiency of the designed trajectory. In addition, a larger transmit power and a relatively smaller number of energy receivers can potentially result in a better harvesting performance. In particular, while ignoring the nonlinear charging process in EH, the linear SHF design is observed to fail in maximizing the truly harvested energy, compared with our proposed design, which confirms the necessity of this work.

It is worthwhile to mention that the introduced concept of turning points and the proved optimal SHF structure is possible to be extended into other UAV trajectory design problems, e.g., in UAV-enabled wireless communications, mobile edge computing and sensing, to facilitate modeling

curving trajectories. In addition, during the approximation of harvested energy from the flying period, we designed a differentiation approach for the approximation of an integral function, see the approximation design from (23) to (33). This tool is very helpful in our design, and has a high potential in addressing other trajectory design problems. Moreover, the methodology of this work in handling the nonlinearity of EH, can be extended to carry out more designs for WPT networks.

Due to space limitation, there are some important issues that are unaddressed in this paper, which are discussed in the following to motivate future work.

- In this paper, we focused on the UAV's WPT operation over a fixed time duration T, during which the UAV is assumed to have sufficient energy supplies. In practice, the UAV's energy consumption and energy efficiency are also important issues. By taking into account the energy consumption models at the UAV (see [7] for fixed-wing UAVs and [8] for rotary-wing UAVs), how to optimize the UAV's trajectory to maximize the energy transfer performance with minimum energy consumption is an interesting problem worth further investigation, which are left for future work.
- Furthermore, this paper assumed that the UAV had perfect knowledge about the locations of fixed GDs and simplified free space channel models, for quantifying the fundamental performance limits of this system and gaining the most essential design insights. In some other application scenarios, the GDs may slowly move on the ground and the LoS channels between the UAV and GDs may be blocked by certain obstacles. To tackle the potential location changes of GDs over time, online trajectory designs by using machine learning tools (e.g., (deep) reinforcement learning) might be necessary. To address the potential LoS blockage, new channel models (such as probabilistic LoS channels and radio map techniques with location-based LoS/NLoS channels [18]) might be adopted. Based on such new models, the trajectory design needs to be revised, and the 3D trajectory optimization might become necessary for further enhancing the performance.

APPENDIX A
PROOF OF LEMMA 1

This lemma can be proved by partitioning the whole time duration T into a sufficiently large number of time portions, each with a sufficiently small length such that during the portion the UAV speed is constant and the trajectory in each portion is either a single point or a straight line.

Denote the length of i-th portion by $\tau_i, i = 1, \cdots, I$ and we have $\sum_{i=1,\cdots,I} \tau_i = T$. In addition, denote by v_i the speed of the UAV at the i-th portion, i.e., $0 \leq v_i \leq V$. In the following, we prove Lemma 1 by showing that within each time portion the UAV trajectory satisfying the maximum speed constraint is equivalent to two trajectories $\{\bar{x}(t), \bar{y}(t)\}$ and $\{\hat{x}(t), \hat{y}(t)\}$ as defined in the lemma.

For each i-th portion, there are in total three cases:

Case 1: the UAV hovers over a given location, i.e., $v_i = 0$. Then, this portion can be directly allocated to $\{\hat{x}(t), \hat{y}(t)\}$, so that $\{\hat{x}(t), \hat{y}(t)\}$ have the same hovering point and the same hovering duration τ_i.

Case 2: the UAV flies from $(x_{i,\mathrm{I}}, y_{i,\mathrm{I}})$ to $(x_{i,\mathrm{F}}, x_{i,\mathrm{F}})$ with speed $v_i = V$. Therefore, this portion is directly allocated to $\{\bar{x}(t), \bar{y}(t)\}$. Hence, the trajectory $\{\hat{x}(t), \hat{y}(t)\}$ does not cover the line from $(x_{i,\mathrm{I}}, y_{i,\mathrm{I}})$ to $(x_{i,\mathrm{F}}, x_{i,\mathrm{F}})$ and is not continuous over topology, i.e., there is not UAV speed limit in $\{\hat{x}(t), \hat{y}(t)\}$.

Case 3: the UAV flies from $(x_{i,\mathrm{I}}, y_{i,\mathrm{I}})$ to $(x_{i,\mathrm{F}}, x_{i,\mathrm{F}})$ with speed $0 < v_i < V$. The length of the portion is $\tau_i = \frac{\sqrt{(x_{i,\mathrm{F}}-x_{i,\mathrm{I}})^2+(y_{i,\mathrm{F}}-y_{i,\mathrm{I}})^2}}{v_i}$. We can let the UAV fly with the maximal speed in $\{\bar{x}(t), \bar{y}(t)\}$ which has the time cost $\bar{\tau}_i = \frac{\sqrt{(x_{i,\mathrm{F}}-x_{i,\mathrm{I}})^2+(y_{i,\mathrm{F}}-y_{i,\mathrm{I}})^2}}{V}$. In addition, we let the UAV in $\{\hat{x}(t), \hat{y}(t)\}$ use the remaining time, i.e., $\hat{\tau}_i = \tau_i - \bar{\tau}_i$, to fly from $(x_{i,\mathrm{I}}, y_{i,\mathrm{I}})$ to $(x_{i,\mathrm{F}}, x_{i,\mathrm{F}})$ with corresponding speed being $\frac{Vv_i}{V-v_i}$. It is shown in Eq.(38) that in i-th portion the WPT performance of $\{x(t), y(t)\}$ and the sum WPT performance of $\{\bar{x}(t), \bar{y}(t)\}$ and $\{\hat{x}(t), \hat{y}(t)\}$ are the same $\forall k = 1, \cdots, K$.

$$
\begin{aligned}
&\underbrace{\int_0^{\tau_i} \mathcal{F}_{nl}\left(Q_k(x_{i,\mathrm{I}} + \frac{x_{i,\mathrm{F}}-x_{i,\mathrm{I}}}{\tau_i}t, y_{i,\mathrm{I}} + \frac{y_{i,\mathrm{F}}-y_{i,\mathrm{I}}}{\tau_i}t)\right) dt}_{\{x(t),y(t)\}} \qquad (38)\\
= \quad & \frac{v_i}{V}\int_0^{\tau_i} \mathcal{F}_{nl}\left(Q_k(x_{i,\mathrm{I}}+\frac{x_{i,\mathrm{F}}-x_{i,\mathrm{I}}}{\tau_i}t, y_{i,\mathrm{I}}+\frac{y_{i,\mathrm{F}}-y_{i,\mathrm{I}}}{\tau_i}t)\right) dt + \frac{V-v_i}{V}\int_0^{\tau_i} \mathcal{F}_{nl}\left(Q_k(x_{i,\mathrm{I}}+\frac{x_{i,\mathrm{F}}-x_{i,\mathrm{I}}}{\tau_i}t, y_{i,\mathrm{I}}+\frac{y_{i,\mathrm{F}}-y_{i,\mathrm{I}}}{\tau_i}t)\right) dt \\
\overset{\substack{v_i t = V t_1 \\ v_i t = \frac{V v_i}{V-v_i} t_2}}{=} \quad & \underbrace{\int_0^{\bar{\tau}_i} \mathcal{F}_{nl}\left(Q_k(x_{i,\mathrm{I}}+\frac{x_{i,\mathrm{F}}-x_{i,\mathrm{I}}}{\bar{\tau}_i}t_1, y_{i,\mathrm{I}}+\frac{y_{i,\mathrm{F}}-y_{i,\mathrm{I}}}{\bar{\tau}_i}t_1)\right) dt_1}_{\{\bar{x}(t),\bar{y}(t)\}} + \underbrace{\int_0^{\hat{\tau}_i} \mathcal{F}_{nl}\left(Q_k(x_{i,\mathrm{I}}+\frac{x_{i,\mathrm{F}}-x_{i,\mathrm{I}}}{\hat{\tau}_i}t_2, y_{i,\mathrm{I}}+\frac{y_{i,\mathrm{F}}-y_{i,\mathrm{I}}}{\hat{\tau}_i}t_2)\right) dt_2}_{\{\hat{x}(t),\hat{y}(t)\}}
\end{aligned}
$$

So far, we have shown that for each portion of $\{x(t), y(t)\}$, we can obtain the corresponding parts of $\{\bar{x}(t), \bar{y}(t)\}$ and $\{\hat{x}(t), \hat{y}(t)\}$ having the same WPT performance as the portion of $\{x(t), y(t)\}$. By repeating the above process for every portion of $\{x(t), y(t)\}$, $\{\bar{x}(t), \bar{y}(t)\}$ and $\{\hat{x}(t), \hat{y}(t)\}$ can be developed while satisfying Lemma 1.

APPENDIX B
PROOF OF LEMMA 2

Problem (P2) is non-convex but satisfies the so-called time-sharing condition in [39]. Therefore, a strong duality holds between problem (P2) and its Lagrange dual problem. Then, problem can be solved via the Lagrange dual method [40].

Denote the Lagrange multipliers for the k-th constraint in (10b) by $\lambda_k \geq 0, k \in \mathcal{K}$. The partial Lagrangian of problem (P2) is given by

$$\begin{aligned}&\mathcal{L}_2\left(\{\hat{x}(t),\hat{y}(t)\},E,\{\lambda_k\}\right)\\ =&(1-\sum\nolimits_{k\in\mathcal{K}}\lambda_k)E+\sum\nolimits_{k\in\mathcal{K}}\lambda_k\bar{E}_k+\int_0^{\hat{T}}\sum\nolimits_{k\in\mathcal{K}}\lambda_k\mathcal{F}_{nl}(Q_k(\hat{x}(t),\hat{y}(t)))dt.\end{aligned} \tag{39}$$

Immediately, we have the corresponding dual function as

$$f_2\left(\{\lambda_k\}\right) = \max_{\{\hat{x}(t),\hat{y}(t)\},E} \mathcal{L}_2\left(\{\hat{x}(t),\hat{y}(t)\},E,\{\lambda_k\}\right) \tag{40}$$

$$\text{s.t. } (\hat{x}(t),\hat{y}(t)) \in \{(x(t_0),y(t_0))|t_0\in\mathcal{T}\},\ \forall t\in[0,\hat{T}]. \tag{41}$$

Clearly, the condition $1-\sum_{k\in\mathcal{K}}\lambda_k = 0$ must be satisfied to guarantee that the function $f_2(\{\lambda_k\})$ is upper-bounded from above, i.e., $f_2(\{\lambda_k\})<\infty$. Then, the dual problem of problem (P2) is given by

$$(\text{DP2}): \max_{\{\lambda_k\}}\ f_2(\{\lambda_k\}) \tag{42a}$$

$$\text{s.t. } 1-\sum\nolimits_{k\in\mathcal{K}}\lambda_k=0,\ \lambda_k\geq 0,\forall k\in\mathcal{K}. \tag{42b}$$

Notice that as strong duality holds between problem (P2) and its dual problem (DP2), we solve problem (P2) by equivalently solving the dual problem (DP2), in which we first obtain the dual function $f_2\left(\{\lambda_k\}\right)$ under any given $\{\lambda_k\}$ by solving problem (40), and then updating $\{\lambda_k\}$ via subgradient-based methods such as the ellipsoid method [36] to find the optimal $\{\lambda_k^*\}$ maximizing $f_2(\{\lambda_k\})$.

First of all, we deteminate the dual function $f(\{\lambda_k\})$. Consider problem (40) under any given $\{\lambda_k\}$ satisfying the constraints in (DP2). As $1-\sum_{k\in\mathcal{K}}\lambda_k = 0$, problem (40) can be decomposed into the following subproblems by dropping the constant term $\sum\lambda_k\bar{E}_k$, each for one time instant $t\in\mathcal{T}$.

$$\max_{\{\hat{x}(t),\hat{y}(t)\}} \quad \sum\nolimits_{k\in\mathcal{K}} \lambda_k \mathcal{F}_{nl}(Q_k(\hat{x}(t),\hat{y}(t))) \tag{43a}$$

$$\text{s.t.} \quad (\hat{x}(t),\hat{y}(t)) \in \{(x(t_0),y(t_0))|t_0 \in \mathcal{T}\},\ \forall t \in [0,\hat{T}]. \tag{43b}$$

As the problem has the same form at different time instant t, we can drop the variable t and reexpress the problem as

$$\max_{\hat{x},\hat{y}} \quad F(\hat{x},\hat{y}) \triangleq \sum\nolimits_{k\in\mathcal{K}} \lambda_k \mathcal{F}_{nl}(Q_k(\hat{x},\hat{y})) \tag{44a}$$

$$\text{s.t.} \quad (\hat{x},\hat{y}) \in \{(x(t_0),y(t_0))|t_0 \in \mathcal{T}\}. \tag{44b}$$

We can obtain the optimal solution by searching the maximal point along the path of $\{x(t),y(t)\}$. As a result, multiple points are searched out as the solution of problem (44a). As the solution has dropped variable t, the optimal solution of problem (P2) will be a hovering behaviour over these points when $\lambda_k = \lambda_k^\star, \forall k \in \mathcal{K}$. By optimally allocating hovering durations on these points, the optimal trajectory of problem (P2) is eventually built. Then, a hovering behaviour of the optimal trajectory to problem (P2) is proved.

APPENDIX C
PROOF OF LEMMA 3

We first address the relationship between the number of hovering points M with K, i.e., $M \leq K$, and subsequently show that the total number M' of the starting, ending and hovering points satisfies $M' \leq K$.

A. At most K hovering points to construct optimal trajectory

Denoted the M hovering points in an optimal trajectory by $(x_1,y_1),\cdots,(x_M,y_M)$ with corresponding positive hovering durations $\mathbf{t} = (\tau_1,\cdots,\tau_M)$. Then, we define a charging matrix $\mathbf{U} = (u_{mk})_{M\times K}$, where $u_{mk} = \mathcal{F}_{nl}(Q_k(x_m,y_m))$ and $\mathbf{u}_m$ is the m-th row of matrix $\mathbf{U}$. Additionally, we denote the harvested energy at GDs during flying period by $\bar{\mathbf{E}} = (\bar{E}_1,\cdots,\bar{E}_K)^T$. Hence, the received energy at GDs during the whole period can be obtained by $\sum_{m=1}^{M}\tau_m\mathbf{u}_m + \bar{\mathbf{E}} = (E_1,\cdots,E_K)^T$. In the following, we prove at most K hovering points can achieve the optimal performance by showing: For an optimal trajectory with $M > \mathbf{rank}(\mathbf{U})$, we can always find a trajectory that achieves the same WPT but with only $\mathbf{rank}(\mathbf{U})$ hovering points.

As $M >$ rank$(\mathbf{U})$, the rows of matrix $\mathbf{U}$ will be linearly dependent, i.e., there exists $s_m \neq 0, m = 1,\cdots,M$ such that $\sum_{m=1}^{M} s_m\mathbf{u}_m = \mathbf{0}^{1\times K}$. Hence, we have the following lemma.

Lemma 4. *For an optimal trajectory with $M > \mathbf{rank}(\mathbf{U})$ hovering points, $\sum_{m=1}^{M} s_m = 0$ holds.*

Proof. It is proved by contradiction while distinguishing following two cases:

Case 1: when $\sum_{m=1}^{M} s_m > 0$, we let $i = \arg\min_{m,s_m>0} \frac{\tau_m}{s_m}$. Then, we delete hovering point i and reallocate the hovering duration to remaining hovering points to obtain a better performance. The hovering duration reallocation is definited as

$$\begin{cases} \tau_j \longrightarrow \tau_j - \frac{\tau_i}{s_i} s_j + \frac{\tau_i}{M-1}(1 - \sum_{j\neq i}(-\frac{s_j}{s_i})), & \text{when } j \neq i\,, \\ \tau_j \longrightarrow 0, & \text{when } j = i\,. \end{cases} \tag{45}$$

Note that the total charging duration does not change, i.e., $\sum_{j\neq i}\left(\tau_j - \frac{\tau_i}{s_i}s_j + \frac{\tau_i}{M-1}(1 - \sum_{j\neq i}(-\frac{s_j}{s_i}))\right) = \sum_{j\neq i}\tau_j + \tau_i$. And $\tau_j - \frac{\tau_i}{s_i}s_j \geq 0$ holds due to $i = \arg\min_{m,s_m>0}\frac{\tau_m}{s_m}$, $1 - \sum_{j\neq i}(-\frac{s_j}{s_i}) > 0$ holds due to $\sum_{m=1}^{M} s_m > 0$ and $s_i > 0$. Thus, the hovering duration in new allocation is still larger than zero. For the new allocation, the received energy is given by

$$\begin{aligned} & \sum\nolimits_{j\neq i}\left(\tau_j - \frac{\tau_i}{s_i}s_j + \frac{\tau_i}{M-1}(1 - \sum\nolimits_{j\neq i}(-\frac{s_j}{s_i}))\right)\mathbf{u}_j + \bar{\mathbf{E}} \\ = \; & \sum\nolimits_{j\neq i}\tau_j\mathbf{u}_j - \frac{\tau_i}{s_i}\sum\nolimits_{j\neq i}s_j\mathbf{u}_j + \sum\nolimits_{j\neq i}\left(\frac{\tau_i}{M-1}(1 - \sum\nolimits_{j\neq i}(-\frac{s_j}{s_i}))\right)\mathbf{u}_j + \bar{\mathbf{E}} \\ \overset{s_i\mathbf{u}_i = -\sum_{j\neq i}s_j\mathbf{u}_j}{=} \; & \sum\nolimits_{m=1}^{M} t_m\mathbf{u}_m + \bar{\mathbf{E}} + \sum\nolimits_{j\neq i}\left(\frac{\tau_i}{M-1}(1 - \sum\nolimits_{j\neq i}(-\frac{s_j}{s_i}))\right)\mathbf{u}_j \\ = \; & (E_1, \cdots, E_K)^T + \sum\nolimits_{j\neq i}\left(\frac{\tau_i}{M-1}(1 - \sum\nolimits_{j\neq i}(-\frac{s_j}{s_i}))\right)\mathbf{u}_j. \end{aligned} \tag{46}$$

Note that each element in vector $\sum_{j\neq i}\left(\frac{\tau_i}{M-1}(1 - \sum_{j\neq i}(-\frac{s_j}{s_i}))\right)\mathbf{u}_j$ is larger than zero. Hence, all GDs are received more energy in the new allocation. Thus, $\sum_{m=1}^{M} s_m > 0$ does not hold.

Case 2: when $\sum_{m=1}^{M} s_m < 0$, we define $i = \arg\max_{m,s_m<0}\frac{\tau_m}{s_m}$ and do the same allocation. In the same way as above, it can be proved there is also an allocation scheme with better performance.

Therefore, $\sum_{m=1}^{M} s_m = 0$ holds in an optimal trajectory when $M > \mathbf{rank}(\mathbf{U})$. □

For an optimal trajectory S.1 with $M > \mathbf{rank}(\mathbf{U})$, the hovering point i can be determined according to $i = \arg\min_{m}\frac{\tau_m}{|s_m|}$. Then, we can obtain a new trajectory S.2 by deleting this hovering point i and re-allocating its hovering duration to the rest hovering points of S.1 following (45). According to (46), as $1 - \sum_{j\neq i}(-\frac{s_j}{s_i}) = 0$, S.1 and S.2 have the same WPT performance, i.e., S.2 is also optimal. By iteratively applying this process of deleting hovering point and re-allocating hovering duration, we finally obtain an optimal trajectory with only $\mathbf{rank}(\mathbf{U})$ hovering points. Note that $\mathbf{rank}(\mathbf{U}) \leq K$. Hence, the statement is proved.

B. Total number M' of starting, ending and hovering points is no more than K points in at least one optimal solution

We prove this statement by distinguishing three different cases: i. the starting and ending points are hovering points, i.e, $M'=M$, where the statement clearly holds according to the proof in Part A. ii. both the starting and ending points are not hovering points, i.e., $M'=M+2$. iii. one of the starting and ending points is a hovering point, i.e., $M'=M+1$. In the following, we provide the proof for the second case, while the third case can be proved in the same way.

If $M' \leq K$, the statement clearly holds. Hence the major difficulty is to prove the statement when $M'=M+2>K$. We denote the starting and ending points of the trajectory by $(x_{\rm I}, y_{\rm I})$ and (x_F, y_F). Similar to the proof in Appendix C-A, we obtain the charging matrix $\mathbf{U}$ based on the M hovering points and M hovering durations with $\sum_{m=1}^{M} \tau_m \mathbf{u}_m + \bar{\mathbf{E}} = (E_1, \cdots, E_K)^T$ holds. In addition, note that the UAV flies along a curve/arc from $(x_{\rm I}, y_{\rm I})$ to (x_1, y_1) and from (x_M, y_M) to (x_F, y_F) with maximum speed V. We define a positive time duration $\delta t > 0$ which is such small that the UAV can be considered as static. By carving up the curve/arc from $(x_{\rm I}, y_{\rm I})$ to (x_1, y_1) at starting point $(x_{\rm I}, y_{\rm I})$ with length $\delta t V$, we can obtain a virtual hovering point $(x_{\rm I}, y_{\rm I})$ with duration δt. In the same way, another virtual hovering point at $(x_{\rm F}, y_{\rm F})$ can be also constructed with hovering duration δt.

Considering both virtual hovering points $(x_{\rm I}, y_{\rm I})$ and $(x_{\rm F}, y_{\rm F})$ as two additional hovering points with hovering duration δt, we therefore update the charging matrix $\mathbf{U}$ and harvested energy from flying period $\bar{E}$ accordingly. As $\mathbf{rank}(\mathbf{U}) \leq K$ and $M' > K$ hold, the rows of matrix $\mathbf{U}$ will be linearly dependent, i.e., there exists $s_m \neq 0, m = 1, \cdots, M'$ such that $\sum_{m=1}^{M'} s_m \mathbf{u}_m = \mathbf{0}^{1\times K}$ and $\sum_{m=1}^{M'} s_m = 0$ holds according to Lemma 4. Based on the discussion in Appendix C-A, through a proper selection of point deletion and the new hovering duration allocation (45), an equal/better performance will be obtained. If the deleted hovering point is originally a hovering point, the deletion will reduce the number of these points to $\mathbf{rank}(\mathbf{U}) \leq K$. If the deleted point is starting point $(x_{\rm I}, y_{\rm I})$ or ending point $(x_{\rm F}, y_{\rm F})$, the deletion will not influence the continuity of the trajectory. Moreover, the length of curve before the first hovering point (x_1, y_1) or after last hovering point (x_M, y_M) will be reduced by $\delta t V$, and the starting or ending point will be updated. By repeating the above process, the length of curve before the first hovering point or after last hovering point is constantly reduced, until M' is less than K or the length of the curve is reduced to 0 within finite repeats (the starting or ending point eventually becomes a hovering points). Meanwhile, the overall performance is not decreased, i.e., the trajectory is still optimal.

REFERENCES

[1] Y. Zeng, R. Zhang, and T.J. Lim, "Wireless communications with unmanned aerial vehicles: Opportunities and challenges," *IEEE Commun. Mag.*, vol. 54, no. 5, pp. 36-42, May 2016.

[2] L. Gupta, R. Jain and G. Vaszkun, "Survey of important issues in UAV communication networks," *IEEE Commun. Surveys Tuts.*, vol. 18, no. 2, pp. 1123-1152, SecondQuarter 2016.

[3] A. Al-Hourani, S. Kandeepan, and S. Lardner, "Optimal LAP altitude for maximum coverage," *IEEE Wireless Commun. Lett.*, vol. 3, no. 6, pp. 569–572, Dec. 2014.

[4] J. Lyu, Y. Zeng, R. Zhang, and T.J. Lim, "Placement optimization of UAV-mounted mobile base stations," *IEEE Commun. Lett.*, vol. 21, no. 3, pp. 604–607, Mar. 2017.

[5] R. Fan, J. Cui, S. Jin, K. Yang, and J. An, "Optimal node placement and resource allocation for UAV relaying network," *IEEE Wireless Commun. Lett.* , vol. 22, no. 4, pp. 808-811, Apr. 2018.

[6] P. Li and J. Xu, "Fundamental rate limits of UAV-enabled multiple access channel with trajectory optimization," *IEEE Trans. Wireless Commun.*, vol. 19, no. 1, pp. 458-474, Jan. 2020.

[7] Y. Zeng and R. Zhang, "Energy-Efficient UAV Communication With Trajectory Optimization," *IEEE Trans. Wireless Commun.*, vol. 16, no. 6, pp. 3747-3760, June 2017.

[8] Y. Zeng, J. Xu, and R. Zhang, "Energy minimization for wireless communication with rotary-wing UAV", *IEEE Trans. Wireless Commun.*, vol. 18, no. 4, pp. 2329-2345, Apr. 2019.

[9] Y. Zeng, R. Zhang and T. J. Lim, "Throughput maximization for UAV-enabled mobile relaying systems," *IEEE Trans. Commun.*, vol. 64, no. 12, pp. 4983-4996, Dec. 2016.

[10] V. Sharma, M. Bennis and R. Kumar, "UAV-assisted heterogeneous networks for capacity enhancement," *IEEE Commun. Lett.*, vol. 20, no. 6, pp. 1207-1210, Jun. 2016.

[11] C. Zhan, Y. Zeng, and R. Zhang, "Energy-efficient data collection in UAV enabled wireless sensor network," *IEEE Wireless Commun. Lett.*, vol. 7, no. 3, pp. 328-331, Jun. 2018.

[12] F. Cheng, S. Zhang, Z. Li, Y. Chen, and N. Zhao, "UAV trajectory optimization for data offloading at the edge of multiple cells," *IEEE Trans. Veh. Technol.*, vol. 67, no. 7, pp. 6732-6736, Jul. 2018.

[13] Y. Hu, Y. Zhu, M. C. Gursoy, and A. Schmeink, "SWIPT-enabled relaying in IoT networks operating with finite blocklength codes." *IEEE J. Sel. Areas Commun.*, vol. 37, no. 2, pp. 1-16, Feb. 2019.

[14] S. Bi, C.K. Ho, and R. Zhang, "Wireless powered communication: Opportunities and challenges," *IEEE Commun. Mag.*, vol. 53, no. 4, pp. 117–125, Apr. 2015.

[15] X. Lu, P. Wang, D. Niyato, and D.I. Kim, "Wireless networks with RF energy harvesting: A contemporary survey," *IEEE Commun. Surv. Tut.*, vol. 17, no. 2, pp. 757-789, Secondquarter 2015.

[16] J. Xu, Y. Zeng, and R. Zhang, "UAV-enabled wireless power transfer: Trajectory design and energy optimization," *IEEE Trans. Wireless Commun.*, vol. 17, no. 8, pp. 5092–5106, Aug. 2018.

[17] Y. Hu, X. Yuan, J. Xu, and A. Schmeink, "Optimal 1D trajectory design for UAV-enabled multiuser wireless power transfer," *IEEE Trans. Commun.*, vol. 67, no. 8, pp. 5674-5688, Aug. 2019.

[18] X. Mo, Y. Huang, and J. Xu, "Radio-map-based robust positioning optimization for UAV-enabled wireless power transfer," *IEEE Wireless Commun. Lett.*, vol. 9, no. 2, pp. 179-183, Feb. 2020.

[19] L. Xie, J. Xu, and R. Zhang, "Throughput maximization for UAV-enabled wireless powered communication networks," *IEEE Internet Things J.*, vol. 6, no. 2, pp. 1690-1703, Apr. 2019.

[20] L. Xie, J. Xu, and Y. Zeng, "Common throughput maximization for UAV-enabled interference channel with wireless powered communications," *IEEE Trans. Commun.*, vol. 8, no. 5, pp. 3197-3212, May 2020.

[21] Y. Wang, M. Hua, Z. liu, D. Zhang, H. Dai, and Y. Hu, "Joint scheduling and trajectory design for UAV-aided wireless power transfer system." in *Proc. International Conference on 5G for Future Wireless Networks*, Springer, Cham, 2019.

[22] Y. Dong, M.J. Hossain, and J. Cheng. "Performance of wireless powered amplify and forward relaying over Nakagami-m fading channels with nonlinear energy harvester," *IEEE Commun. Lett.*, vol. 20, no. 4, pp: 672-675, 2016.

[23] M. Hua, C. Li, Y. Huang, and L. Yang, "Throughput maximization for UAV-enabled wireless power transfer in relaying system." in

[24] Y. Liu, K. Xiong, Q. Ni, and P. Fan, "UAV-Assisted Wireless Powered Cooperative Mobile Edge Computing: Joint Offloading, CPU Control, and Trajectory Optimization." *IEEE Internet Things J.*, vol. 7, no. 4, pp: 2777-2790, Apr. 2019.*Proc. IEEE International Conference on Wireless Communications and Signal Processing (WCSP), 2017.*

[25] Y. Liu, K. Xiong, Q. Ni, and P. Fan, "UAV-Assisted Wireless Powered Cooperative Mobile Edge Computing: Joint Offloading, CPU Control, and Trajectory Optimization." IEEE Internet Things J.*, vol. 7, no. 4, pp: 2777-2790, Apr. 2019.*

[26] V., Christopher R., and G. D. Durgin, "Harvesting wireless power: Survey of energy-harvester conversion efficiency in far-field, wireless power transfer systems." IEEE Microw. Mag. *15.4, 2014, pp:108-120.*

[27] B. Clerckx, R. Zhang, R. Schober, D. W. K. Ng, D. I. Kim, and H.V. Poor, "Fundamentals of wireless information and power transfer: From RF energy harvester models to signal and system designs," IEEE J. Sel. Areas Commun. *, vol. 37, no. 1, pp. 4-33, Feb. 2019.*

[28] E. Boshkovska, D.W.K. Ng, N. Zlatanov, and R. Schober, "Practical non-linear energy harvesting model and resource allocation for SWIPT systems," IEEE Commun. Lett.*, vol. 19, no. 12, pp: 2082-2085, 2015.*

[29] J. Park, H. Lee, S. Eom, and I. Lee, "UAV-aided wireless powered communication networks: Trajectory optimization and resource allocation for minimum throughput maximization." IEEE Access*, vol. 7, pp: 134978-134991, 2019.*

[30] P. Zhang, Z. Wang, Q. Zhang, Y. Liu, X. Wan and Z. Fan, "Max-min Placement optimization for UAV Enabled Wireless Powered Networks with Non-linear Energy Harvesting Model," 2020 IEEE 5th International Conference on Cloud Computing and Big Data Analytics (ICCCBDA), Chengdu, China, 2020, pp. 436-439.

[31] B. Clerckx and E. Bayguzina, "Waveform design for wireless power transfer," IEEE Trans. Signal Proces.*, vol. 64, no. 23, Dec. 2016.*

[32] Y. Hu, X. Yuan, T. Yang, B. Clerckx, and A. Schmeink, "On the convex properties of wireless power transfer with nonlinear energy harvesting," IEEE Trans. Veh. Technol.*, accepted. [Online]. Available: arXiv:1912.04785.*

[33] D. Ho, E.I. Grøtli, P.B. Sujit, T.A. Johanson, and J.B. Sousa, "Optimization of wireless sensor n network and UAV data acquisition," J. Intell. Robot Syst. *vol. 78, pp. 159–179, 2015.*

[34] K. Dogancay, "UAV Path Planning for Passive Emitter Localization," IEEE Trans. Aero. Elec. Sys.*, vol. 48, no. 2, pp. 1150-1166, Apr. 2012.*

[35] F. Kendoul, Y. Zhenyu and K. Nonami, "Embedded autopilot for accurate waypoint navigation and trajectory tracking: Application to miniature rotorcraft UAVs," in Proc. IEEE ICRA*, Kobe, 2009, pp. 2884-2890.*

[36] S. Boyd. EE364b Convex Optimization II, Course Notes*, accessed on Jun. 29, 2017. [Online]. Available: http://www.stanford.edu/class/ ee364b/*

[37] H.A. Abdulkarim and I.F. Alshammari, "Comparison of algorithms for solving traveling salesman problem." Int. J. Eng. Adv. Tech.*, vol.4, no.6, pp.76-79, Aug 2015.*

[38] S. Bubeck, "Convex optimization: Algorithms and complexity." Foundations & Trends in Machine Learning*, 2014, 8(3-4):231-357. Available: https://arxiv.org/pdf/1405.4980v2.pdf*

[39] W. Yu and R. Lui, "Dual methods for nonconvex spectrum optimization of multicarrier systems," IEEE Tran. Commun.*, vol. 54, no. 7, pp. 1310–22, Jul. 2006.*

[40] S. Boyd and L. Vandenberghe, "Convex Optimization," Cambridge, U.K.*: Cambridge Univ. Press, 2004.*